EXPERIMENTAL AND NUMERICAL STUDY OF THE EFFECT OF DESIGN AND PROCESSING PARAMETERS ON SPRING-IN IN COMPOSITE PARTS

by
Kenan Çınar
B.S., in M.E., Celal Bayar University, 2005

Submitted to the Institute for Graduate Studies in
Science and Engineering in partial fulfillment of
the requirements for the degree of
Master of Science

Graduate Program in Mechanical Engineering
Boğaziçi University
2008

ACKNOWLEDGEMENTS

I would like to thank my thesis advisor, Asst. Prof. Nuri Ersoy for his support and advise by all means.

Also, I would like to thank my friends for their support.

Finally, there are no word to express my gratitude for the love and support provided by my family.

ABSTRACT

EXPERIMENTAL AND NUMERICAL STUDY OF THE EFFECT OF DESIGN AND PROCESSING PARAMETERS ON SPRING-IN IN COMPOSITE PARTS

Residual stresses appearing during cure of thermoset composite laminates lead to distortions such as spring-in. The dimensional changes in the produced parts cause the parts not to mate closely with the other parts in the assembly. To solve the problems regarding dimensional changes in the part, a trial and error approach is preferred in applications but this method is very expensive and time consuming in the production of large components. Therefore distortions should be predicted closely before manufacturing parts.

In this study, the effect of design and processing parameters such as stacking sequence, part thickness, and corner radius on spring-in were examined experimentally and numerically. A U-shaped steel mold was manufactured to fabricate L-shaped composite laminates. The composite material used was AS4/8552 prepreg system. The mold (tool) was heated by plate heaters, not by hot air, which is different from autoclave systems.

To predict spring-in value for L-shaped composite laminates due to the cure process, a 2-D finite element model was used. The finite element model consists of three steps: viscous state, rubbery state, and glassy state. For the deformation of the parts, generalized plane strain elements were preferred in the first and second step and in the third step generalized plane stress condition was used.

ÖZET

KOMPOZİT PARÇALARDA DİZAYN VE YÖNTEM PARAMETRELERİNİN SPRING-IN ÜZERİNE ETKİLERİNİN DENEYSEL VE SAYISAL İNCELENMESİ

Katmanlı termoset kompozitlerin pişmesi sırasında oluşan artık gerilmeler açi kapanması gibi çarpılmalara neden olur. Üretilen parçalardaki bu ölçüsel değişmeler parçaların montaj içindeki diğer parçalarla sıkı olarak birleşememesine neden olur. Parçalardaki ölçüsel değişmelerle ilgili olan bu problemleri çözmek için uygulamada deneme yanılma yaklaşımı tercih, edilir fakat bu yöntem büyük parçaların uretilmesinde çok pahalı ve zaman harçayıcıdır. Bu nedenle parçalar üretilmeden önce çarpılmalar yakın bir tahminle belirlenmelidir.

Bu çalışmada istif oryantasyonu, parça kalınlığı ve köşe yarı çapı gibi tasarım ve yöntem parametrelerinin spring-in üzerindeki etkileri deneysel ve sayısal olarak incelenmiştir. L şeklindeki katmanlı kompozitleri üretmek için U şeklinde çelik kalıp üretildi. Kullanılan kompozit malzemesi AS4/8552 prepreg sistemiydi. Kalıp, otoklav sistemlerinden farklı olarak hava ile değil levha ısıtıcılarla ısıtıldı.

Pişme işlemi sırasında, L şeklindeki kompozit katmanlarin spring-in değerini tahmin etmek için 2 boyutlu sonsuz elemanlı model kullanıldı. Sonsuz elemanlı model üç adımdan oluşuyordu: sıvı halinde, lastik halinde ve cam halinde. Parçaların şekil değiştirmesi için, birinci ve ikinci adımda genelleştirilmiş düzlem şekil değiştirme elemanı tercih edilmiş ve üçünçü adımda genelleştirilmiş düzlem gerilme durumu kullanılmıştır.

TABLE OF CONTENTS

LIST OF FIGURES

LIST OF TABLES

LIST OF SYMBOLS/ABBREVIATIONS

^oC	Celsius
^oF	Fahrenheit
GPa	Gigapascal
mm	Millimeter
MPa	Megapascal
θ	Initial part angle
$\Delta\theta$	Total spring-in angle
$\Delta\theta_{CS}$	Cure shrinkage component of spring-in
$\Delta\theta_{CTS}$	Thermal component of spring-in
$\Delta\theta_{Non\text{-}Thermoelastic}$	Non-thermoelastic component of spring-in
$\Delta\theta_{Stress\ Grad}$	Stress gradient
$\Delta\theta_{Thermoelastic}$	Thermoelastic component of spring-in
$\Delta\theta_{Vf\ Grad}$	Material property gradient
ΔT	Change in temperature
α_{ii}	Coefficient of thermal expansion in principal direction
α_c	In-plane coefficient of thermal expansion
α_r	Through thickness coefficient of thermal expansion
ε_{11}	Fiber direction strain
ε_{22}	Transverse direction strain
ε_{33}	Through thickness direction strain
ε_{ii}^{cure}	Cure shrinkage strains in principal directions
ε_c	In-plane chemical shrinkage strain
ε_r	Through thickness chemical shrinkage strain
ß	Angle between the arms
γ_{ij}	In-plane shear stresses
υ_{ij}	Poisson ratios
A_T	Total area of image
E_{11}	Elastic modulus in fiber direction
E_{22}	Elastic modulus in transverse direction

E_{33}	Elastic modulus through thickness
G_{ij}	In-plane shear modulus
N_f	Number of fiber
r_f	Radius of a fiber
T_f	Curing temperature
T_o	Room temperature
V^{bleed}	Volume of bleeded resin
V_f	Fiber volume fraction
V^{fibers}	Volume of fibers
V^{resin}	Volume of resin

AS4/3501-6	Low viscous Prepreg Material
AS4/8552	High viscous Prepreg Material
COMPRO	Two dimensional finite element code
CPRESS	Autoclave pressure
CSHEAR	Tool-part interface shear stress
COPEN	Opening between part and tool
CSLIP	Relative slip between part and tool
CTE	Coefficient of thermal expansion
FE	Finite element
FEM	Finite element model
FEP	Fluorinated ethylene propylene
FEBM	Finite element based micromechanics
MRCC	Manufacturer recommended cure cycle
RTM	Resin transfer molding
R15	The part with 15 mm radius
R25	The part with 25 mm radius
UD	Unidirectional parts
XP	Cross-ply parts

1. INTRODUCTION

There has been a rapid growth in the use of fiber reinforced composites in engineering applications such as aerospace industry. The rapid growth has been achieved mainly by the substitution of traditional materials, primarily metals by composite materials. The reason for the replacement, in some respects, is that composite materials have superior properties as they are compared to high strength engineering materials. The main advantages of composite materials are their higher specific modulus (the modulus per unit weight) and specific strength (strength per unit weight) which means that the weight of components can be reduced. Hence, decrease in the weight of parts results in efficiency and energy savings.

Basically, reinforcing fiber and a matrix resin form a fiber-reinforced composite. These two different structures are bonded together with interfaces which play a major role in the mechanical and physical properties of composite materials. Reinforcement of the matrix is accomplished by the fibers which carry the majority of the loading and which inherently have superior properties to the bulk fiber material. On the other hand, the matrix represents the binding material of the composite which supports and protect the fibers. Also, it separates the fibers and stops cracks from propagating directly from fiber to fiber.

In laminated composite materials, the matrix material can be either thermosets or thermoplastics. In thermosetting polymers, the liquid resins are converted into hard brittle solids by chemical cross-linking reactions [1]. Because of cross-linking which leads to formation of a tightly bound three-dimensional network of polymer chains, thermosetting polymers do not melt on heating. Also, thermosetting resins are usually isotropic.

Unlike thermosetting resins, thermoplastics are not cross-linked so they can be reformed with the application of heat and pressure. Thermoplastics are made-up of linear molecular chains. They derive their strength from the high concentration of molecular entanglements. When thermoplastics are heated, disentanglement and a change from a rigid solid to a viscous liquid occur. Thermoplastics have anisotropic properties depending on the conditions during solidification.

The autoclave processing is a very common method in the engineering applications, especially in the aerospace industry. In this process, prepregs composed of thermosetting resins and the reinforcing fibers are used. By using a prepreg, the proportion of resin to fiber is kept constant within very close limits and fiber orientation is also easily controlled. In the process, prepregs are cut, laid down in the desired fiber orientation on a tool, and then peel ply is applied on the laminate. Peel-ply allows excess resin to pass through it and become absorbed in the bleeder material. If a smooth finished surface is desired, a release film should be used. The next layer to be added is the breather, which provides two important functions. First, breather insures the vacuum is distributed evenly within the bag. Second, it absorbs excess resin from the laminate. Finally, a vacuum bag is applied, which covers all the layers. After vacuum bagging, for curing and consolidation of the laminate heat and pressure are applied. A schematic representation of the vacuum bagging process is presented in Figure 1.1.

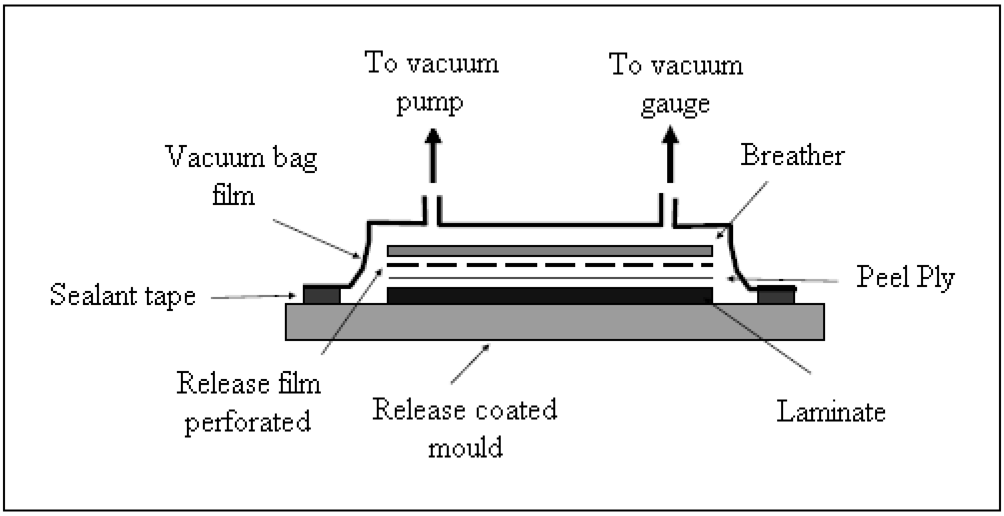

Figure 1.1. Vacuum bagging for prepreg lay-up process.[2]

1.1. Problem Statement

In the production of composite materials, observations show that the final shape of the parts is not same as the mold shape after the process, which in turn cause problems during and after the assembly of parts due to poor contact between mating surfaces. The solution of this problem is very complex because the absolute magnitude of the spring-in is difficult to predict and is often changeable in production. In the applications a trial and error approach is preferred to solve the problems but this method is very expensive and time consuming in the production of large components. If the spring-in is predicted closely in advance trial and error expenses are prevented. To understand the spring-in, first of all, the mechanisms behind it should be considered.

Residual stresses during cure of composite laminates lead to spring-in and warpage. Residual stresses are defined as the stress which remains after the cause of stress (external load, heat gradient) has been removed. In the case of metallic parts, residual stresses can appear during welding and cold drawing applications. In composite structures, residual stresses can be grouped into two different length scales: micro-scale and macro-scale. In both scales, the residual stresses are the result of chemical shrinkage and volumetric change build up by temperature change.

At the micro-scale (fiber scale), mostly, residual stresses can arise from the mismatch of thermal expansion between polymeric resin and the fibers and resin cure shrinkage [3]. Thermal expansion coefficient of fiber is much smaller than the resin. This difference causes the resin to tend to shrink much more than the fibers when the material is cooled to room temperature. The fibers resist to the shrinkage of the resin due to the well-bonded structure of them, therefore, residual stresses are induced. Residual stresses at this scale do not cause significant shape distortions on the part due to very small scale; therefore, residual stresses on the fiber-matrix level can be neglected in the calculations. For example during cooling of cured thermoset part, since the coefficient of Thermal Expansion (CTE) of the matrix resin is much higher than the fiber, tensile residual stresses will be generated in the resin and compressive residual stresses will be generated in the fibers. However since these stresses are balanced and will not result in any distortion in balanced symmetric flat laminates.

However the difference in the CTEs of matrix and the resin will cause differential CTEs of the laminate in the in-plane (matrix dominated) and through-the-thickness directions. This does not cause any distortion in balanced symmetric flat laminates either.

However in curved sections, this results in a reduction in enclosed angles of composite laminates which is often called spring-in. Geometry of spring-in of an enclosed angle is represented in Figure 1.2. A curved laminate has a circumferential coefficient of thermal expansion that is smaller than the coefficient in the thickness direction. The arc length along the circumferential direction is maintained due to stiff fibers while the thickness is reduced. This results in a reduction in the enclosed angle.

During autoclave processing of fiber-reinforced polymer composite structures besides differential thermal expansion between fibers and the matrix, there are other factor that affect spring-in such as resin cure shrinkage, tool-part interaction and corner consolidation are the main reasons for residual stresses build up in the part.

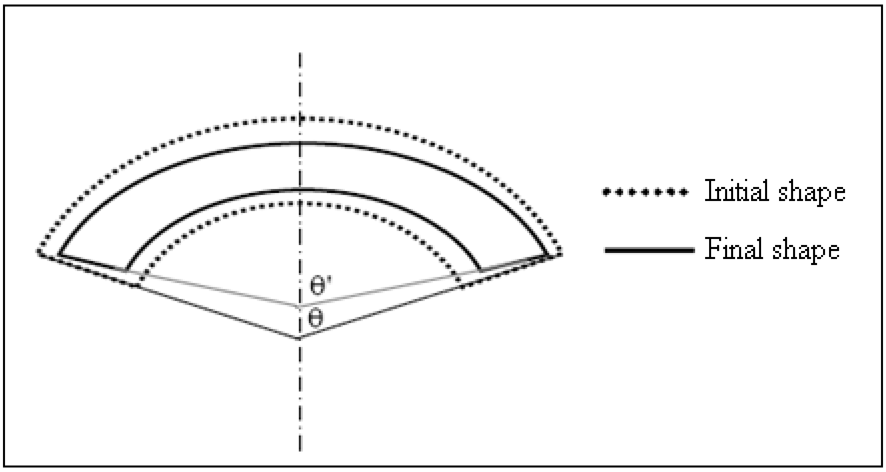

Figure 1.2. Geometry of spring-in of an enclosed angle.[1]

Residual stresses build up on macro-scale (ply-scale) have received much more attention then micro-scale residual stresses due to the fact that such stresses at this level have the largest effect on shape distortions, even laminate cracks and delamination may occur. The main reasons for their presence are anisotropic behavior of individual plies and interaction between tool and part [1]. If we look at the development of residual stresses at the ply level it can be seen that chemical shrinkage along the fiber direction is smaller than the transverse direction, which results in residual stresses between plies. Same phenomenon is valid for tool part-interaction. In industrial applications, generally coefficient of thermal expansion (CTE) of tool is higher than the part CTE, therefore, significant fiber direction stresses (tension stresses) build up during curing.

Besides the difference of the CTEs in the in-plane and through-the-thickness directions, the other source of residual stresses such as corner consolidation, fiber volume fraction gradients, prepreg variability, gradients in the temperature, and laminate consolidation will now be explained in more detail.

1.1.1. Mechanisms Leading to Spring-in

1.1.1.1. Corner Consolidation. For female tooling, if the prepregs do not slip fully, the bag side fibers at the corner counter the most of the pressure so that there would be tensile stresses on the bag side fibers. These stresses are locked in as the part cures, resulting an increase of spring-in, in Figure 1.3. Moreover, the excess resin flows to the corner of the laminate from the arms of the laminate, causing corner thickening, which have an effect on spring-in.

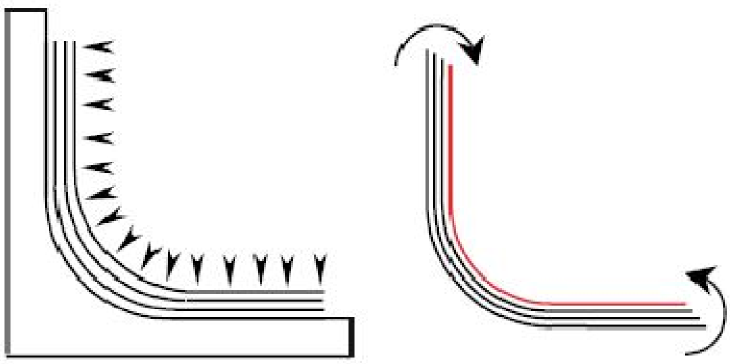

Figure 1.3. Fiber stress due to corner consolidation [4]

1.1.1.2. Fiber volume fraction gradients. Using breather leads to fiber volume fraction gradients in composites. Bag side fiber volume fraction generally can be higher than the tool side one when breather is used. Breather starts to absorb the excess resin of upcoming plies firstly so the resin amount is decreased in the bag side. Fiber volume fraction gradients causes gradients in CTE which change the degree that the part springs-in.

1.1.1.3. Gradients in the Temperature. As the thickness of the parts is increased, the temperature gradients increase since the contact area between the tool and the part heats firstly then the heat spread through the thickness. This may result in differential curing of the part building residual stresses.

<u>1.1.1.4. Tool-part interaction</u>. Manufacturers, generally, use steel or aluminum tools in their productions because these materials have good thermal conductivity and low cost. However these tooling materials have substantially greater thermal expansion than the composite parts. When the tooling material and the composite plies are subjected to a temperature ramp and an autoclave pressure, a shear interaction between tool and part builds up which places the laminate in tension. As this occurs at the early stages of curing, the resin is uncured state and plies distant from the tool are not subjected to same stretching as those adjacent to the interface. This non-uniform stress distribution is fixed in as the resin cures. After process completion, the composite part warps or springs-in from the tool [1, 5, 6]. Mechanism of warpage in flat laminates due to tool-part interaction is presented in Figure 1.4.

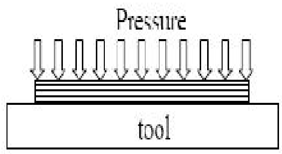 a) Thermal expansion of tool is communicated to the laminate by interfacial shear stresses. This causes tensile stresses in the laminate.	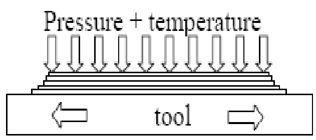 b) The laminate is very soft in shear so plies distant from the tool are not expanded to the same rate as those close to the tool. The resulting stress gradient is locked in when the pre-preg cures.	 c) Bending occurs when stresses are released.

Figure 1.4. Mechanism for warpage due to tool-part interaction [7]

In male tooling, inner surface of the parts interacts with the tool surface, so tensile stress occurs in the inner surface. These tensile stresses at the corner of the parts cause the arm of the parts to deform towards each other when the parts are removed from the tool after curing and this results in an increase in spring-in angle. In contrast, in female tooling such tensile stresses take place in the outer surface of the part and force the arms of the part bend towards the tool as the part released from the tool. Therefore, tool-part interaction in female tools reduces spring-in angle.

Spring-in is not only the result of differential thermal expansion between the fibers and the matrix, but also there may be some other parameters such as part angle, thickness, lay-up, flange length, corner radius, and cure cycle. Actually, these parameters act collectively, even though, the effect of some of these parameters on spring-in is unclear. Moreover, some of them contribute to the spring-in much more on the other hand, the others have little effect on total spring-in.

The source of residual stresses can be divided into two groups: thermoelastic and non-thermoelastic. Thermoelastic spring-in ascribe to shape change due to the mismatch of thermal expansions in the in-plane and through-the-thickness directions. It is reversible when the laminate is heated to the process temperature. In contrast, the non-thermoelastic spring-in is non-reversible. It can be referred to phenomena developing during the cure, such as cure shrinkage, consolidation, tool-part interaction, and gradients in the temperature.

As a result, it is unavoidable that residual stresses are generated within laminated composite materials, resulting in shape distortions like spring-in. In the following section, previous studies regarding to parameters which affect spring-in are presented.

1.2. Literature Review

This section presents an overview of previous experimental and numerical studies which indicate that spring-in may be strongly affected by a number of factors such as material anisotropy, cure shrinkage, cure cycle, tool part-interaction, corner consolidation, lay-up, part angle, corner radius, thickness, flange length, and fiber volume fraction gradients.

1.2.1. Experimental Studies

1.2.1.1. Material Anisotropy, Cure Shrinkage and Part Angle. The main compulsive forces behind the residual stress within the composite are thermal expansion anisotropy and resin cure shrinkage [8]. An equation for predicting the spring-in of angled parts has been proposed by Radford and Diefendorf [9]. This simple formula includes the anisotropy of thermal expansion, cure shrinkage and the part angle of the mold.

$$\Delta\theta_{CTE} = \theta\left(\frac{(\alpha_c-\alpha_r)\Delta T}{1+\alpha_r\Delta T}\right) \tag{1.1}$$

$$\Delta\theta_{CS} = \theta\left(\frac{\varepsilon_c-\varepsilon_r}{1+\varphi_r}\right) \tag{1.2}$$

$$\Delta\theta = \theta[\left(\frac{(\alpha_c-\alpha_r)\Delta T}{1+\alpha_r\Delta T}\right) + \left(\frac{\varepsilon_c-\varepsilon_r}{1+\varphi_r}\right)] \tag{1.3}$$

where;

$\Delta\theta$: total spring-in angle included the thermal and cure shrinkage component of spring-in,

$\Delta\theta_{CTE}$: thermal component of the spring-in angle,

$\Delta\theta_{CS}$: cure shrinkage component of the spring-in angle,

θ: initial part angle,

α_c: in-plane coefficient of thermal expansion,

α_r: through thickness coefficient of thermal expansion,

ε_c: in-plane chemical shrinkage strain,

ε_r: through thickness chemical strain,

ΔT: change in temperature.

Huang and Yang [10] performed some experiments to analyze the effect of mold angle on spring-in. The samples were varying with the angle of 45°, 75°, 90°, 135°, and 165°. They observed that the spring-in angle significantly increased as the part angle decreased. The experimental data had greater (nearly 14%) spring-in than the predicted one. They used Equation (1.3) in their numerical analysis. The results of this study indicate that part angle, cure shrinkage and material anisotropy are responsible for the spring-in.

Yoon and Kim [11] analyzed the effect of thermal anisotropy and the chemical shrinkage of epoxy on the process induced deformation of carbon/epoxy composite laminates. They measured the spring-in angle of L sectioned laminates of various angle plies and compared with the predicted ones. To express the angle change of curved parts due to thermal anisotropy and cure shrinkage, they use the equations (classical lamination theory) below;

$$\Delta\theta_{CTE} = \int_{Tf}^{To} \theta\{\alpha_r(T) - \alpha_c(T)\}dT \tag{1.4}$$

$$\Delta\theta_{CS} = \theta(\varepsilon_r - \varepsilon_c) \tag{1.5}$$

where;

$\Delta\theta_{CTE}$: thermal component of spring-in angle,

$\Delta\theta_{CS}$: chemical component of spring-in,

θ : the part angle of curved laminate,

α_r : through thickness CTE,

α_c : in plane CTE,

T_f : curing temperature,

T_o : room temperature,

ε_r : through thickness chemical strains and

ε_c : in-plane chemical strains.

Their predicted spring-in values were well confirmed by experimental data although the predicted ones were smaller than the experimental ones. They concluded that the main sources of spring-in in curved section were the difference between the through-the thickness and in-plane thermal expansion coefficients of plies and chemical cure shrinkage.

Radford and Rennick [4] studied the thermoelastic and non-thermoelastic behavior of laminated composite materials. Thermoelastic deformations refer to reversible shape distortions; the mismatch of coefficients of thermal expansion in the fiber and transverse directions leads to thermoelastic shape distortions. On the other hand, the non-thermoelastic ones are irreversible when the part is reheated to the process temperature. Change of the spring-in angle as a result of applied temperature is presented in Figure 1.5. The driving forces behind the non-thermoelastic deformations are mainly; cure shrinkage, tool-part interaction, and consolidation. Therefore, they reformulated the Equation (1.3) and described the total spring-in, which covers the concepts of material anisotropy, stress gradients, and material property gradients by;

$$\Delta\theta = \Delta\theta_{Thermoelastic} + \Delta\theta_{Non-Thermoelastic} \tag{1.6}$$

$$\Delta\theta_{Thermoelastic} = \left\{\left[\left(\frac{d\theta}{dT}\right)_{Aniso} + \left(\frac{d\theta}{dT}\right)_{Vf\ Grad}\right].\Delta T\right\} \tag{1.7}$$

$$\Delta\theta_{Non-Thermoelastic} = \left\{\theta\left[\frac{\varepsilon_c-\varepsilon_r}{(1+\varepsilon_r)}\right]_{Aniso} + \Delta\theta_{Vf\ Grad} + \Delta\theta_{Stress\ Grad}\right\} \tag{1.8}$$

where;

$\Delta\theta$: total spring-in angle,

$\Delta\theta_{Thermoelastic}$: thermoelastic component of spring-in,

$\Delta\theta_{Non-Thermoelastic}$: non-thermoelastic component of spring-in,

ε_c: in-plane chemical shrinkage strain,

ε_r: through thickness chemical strain,

$\Delta\theta_{Vf\ Grad}$: material property gradient,

$\Delta\theta_{Stress\ Grad}$: stress gradients such as tool-part interaction.

θ: initial part angle,

ΔT: change in temperature.

In their research, Radford and Rennick [4] found that spring-in angle was greater for smaller part angle, like Huang and Yang [9] although the non-thermoelastic component was more effective than the thermoelastic ones.

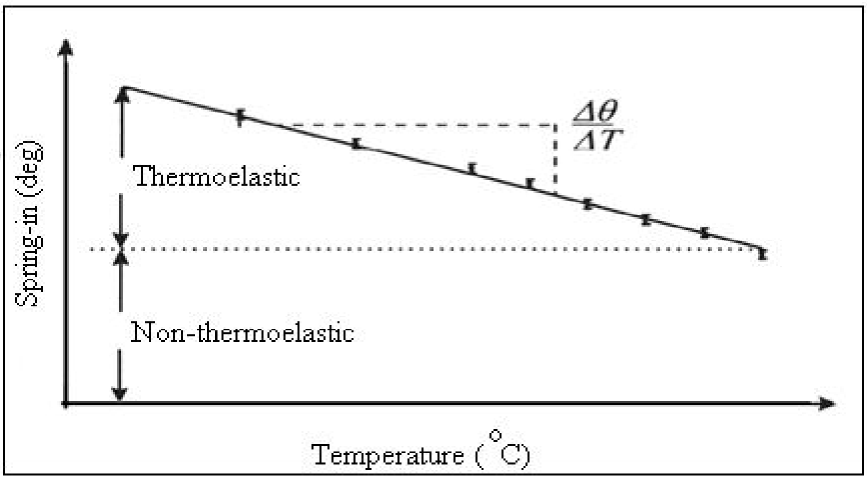

Figure 1.5 Change of the spring-in angle as a result of applied temperature.

1.2.1.2. Tool-Part Interaction. Tool-part interaction is non-thermoelastic, namely, it is irreversible. In his research Garstka [1] indicated that the curvature of a flat part did not change during reheating the part because the curvature is due to tool-part interaction stresses locked-in during curing. He also observed that cross ply samples $[0/90]_s$ had larger curvatures than unidirectional ones $[0]_4$. This was ascribed to the stress decay in the transverse direction plies during early states of cure. The stress decay causes stress gradients through the thickness.

Fernlund *et al*. [3] studied the effect of tool surface and tool material on the spring-in of the parts. They used male tool in their experimental setup. For the tooling surface, they used release agent and release agent + FEP release film. They observed that there was a significantly greater spring-in if the tooling material processed without the FEP sheet. Regarding to tooling material in their research, aluminum tooling had more spring-in than steel tooling if 1-hold cure cycle was performed. This could be attributed to the difference of the coefficient of thermal expansion between steel and aluminum. The thermal expansion coefficient of aluminum is nearly twice of thermal expansion coefficient of steel. Inner surface of the parts interacts with the tool surface in male tooling, so tensile stress occurs in the inner surface. These tensile stresses at the corner of the parts cause the arm of the parts to deform towards the each other when the parts are removed from the tool after curing and this results in an increase in spring-in angle [12].

To minimize the value of spring-in in his analytical and experimental study, Benzie [13] concluded that the performance of steel was better than the aluminum due to its lower CTE.

In another research of Fernlund *et al.* [8], they compared the results of their numerical study (COMPRO) with their experimental study, which was about the tool-surface condition on spring-in. The tool used was a male tool. For one (350 ^{o}F) hold cure cycle, a tool surface without release agent had lower spring-in than a tool surface with release agent. On the other hand, the tool surface with release agent gave lower spring-in as compared to the tool without release agent in two-stage cure cycle (275 and 350 ^{o}F). The COMPRO predictions and the measured values were close together in both cure cycle.

1.2.1.3. Cure Cycle. A cure cycle is often presented as the profile of temperature used to initiate cure within the laminate and bring it to completion. Two typical cure cycles are shown in Figure 1.6 [3]. In vacuum bagging processes, pressure and vacuum may be applied simultaneously with a temperature profile. Increasing the temperature to a set point at a specific rate, holding the temperature until the part has cured to a reasonable extent, and then cooling the part to the room temperature constitute a cure cycle. The first dwell is for the consolidation of the laminate and the second dwell is for the curing of the resin.

Curing of thermosetting composites is required more attention than the thermoplastic composites due to cross-linking reactions which takes place in thermosetting polymers. The thermosetting materials cannot be reshaped [14]. The liquid state of thermosetting matrix at room temperature alters to become a solid when subjected to heat. The properties of liquid resin and a solid resin are different; for example, the specific volume of a liquid and solid resin is not same and this results a cure shrinkage strain. These different properties of thermosetting resin during the process result in shape distortions.

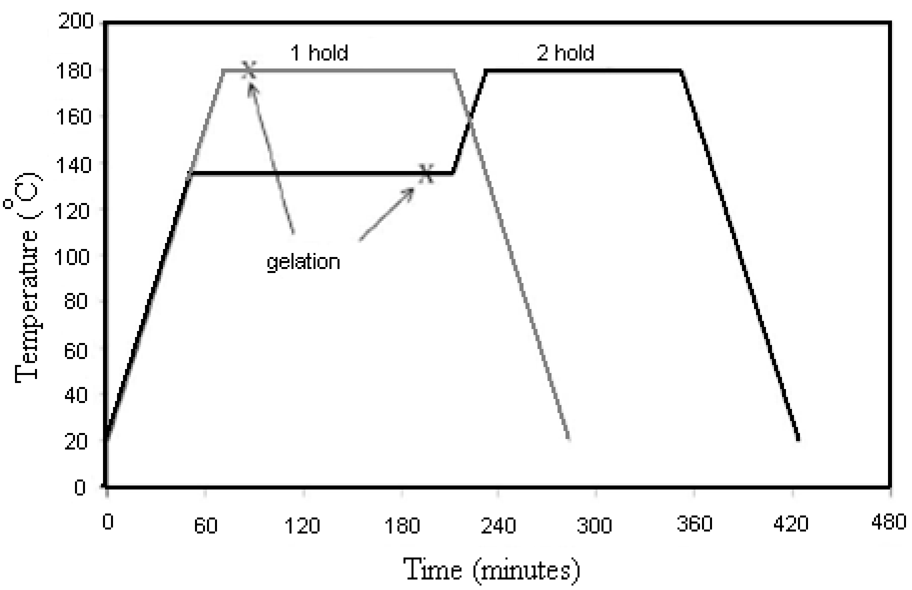

Figure 1.6 A typical one and two hold cure cycle. [3]

Ersoy *et al* [15] adopted a cure quench technique to analyze the development of spring-in angle during cure of AS4/8552 thermosetting composite. In their experiments, the specimens quenched before vitrification had more spring-in angle than the samples quenched after vitrification. According to their explanation, in the rubbery state (before the glass transition temperature) the thermal expansion coefficient of the part was larger than the coefficient of thermal expansion in the glassy state; therefore to quench the samples in the rubbery state caused the samples to shrink more, in turn, more spring-in was inevitable. They also observed that the thermoelastic component of spring-in was %50 of the final spring-in, the remaining is the non-thermoelastic component mainly due to cure shrinkage. Moreover, they concluded that the cooling rate did not affect the final spring-in angle of the quenched specimens.

In their study, Ferlund and Albert [3], indicated that the specimens processed by a two-hold cure cycle exhibited a larger spring-in than the samples cured by a one-hold cycle. In the work of Ferlund *et al* [8], the two hold-cure cycle with release agent on the tool gave %15 greater spring-in than one-hold cure cycle with release agent on the tool and %50 greater spring-in without release agent on the tool. The results of their numerical and experimental studies were quite close to each other.

Svanberg and Holmberg [16] performed their experiments by RTM (resin transfer molding) method, so they used Araldite LY5052/Hardener HY5052 for resin and Hexcel 7781-127 glass wave for fiber. This production method is different from the prepreg layup method. In this method, the mixture of resin and fibers are injected the mold consists of two rigid mould halves (the female and male molds) and then the mold is heated. They observed that increase in the cure temperature led more spring-in because a high cure temperature contributed to larger thermal strains and higher degree of cure. This means that the stress level and corresponding frozen strain at vitrification is higher at higher in-mold cure temperature. It was also found that the cooling rate did not have any significant effect on spring-in.

<u>1.2.1.4. Thickness of the Composite</u>. According to first simple equation (Eq. (1.3)), the thickness of parts does not affect the spring-in phenomena but studies show that the effect of thickness is inevitable. Radford and Rennick [5] performed some experiments to investigate the effect of thickness on the spring-in angle. It was found that the thicker specimens gave smaller spring-in if compared to thinners ones and thermoelastic component of distortion did not affect the spring-in. Non-thermoelastic component was responsible for the different spring-in values for parts with different thickness. According

to them, the explanation of the relationship between thickness and spring-in was that the thicker parts were stiffer than the thinner ones so the thicker parts could better counter residual stresses due to tool-part interaction or cure shrinkage.

In his study, Garstka [1] observed that even the spring-in thermoelastic component of spring-in increased slightly with the increased part thickness. He attributed the fact to the corner-bridging effect which is the result of consolidation occurring in the early stages of curing. This effect limits the plies to shear and causes the pressure to reduce at the corner, hence the resin flows at the corner. In the experimental data, it is shown that corner-bridging mechanism was more effective in the thicker samples. This means that there is more resin at the corner of the samples so the thermal expansion will be higher, therefore it causes more spring-in.

Wisnom *et al* [17] performed shear-lag analysis in their study. In the shear-lag analysis, it was assumed that the material sheared to maintain the same arc length in the rubbery state whereas in the "stiff in shear" assumption, which is implied on Equation. (1.3), there was no shear in the material and spring-in will built-up for maintaining the same arc length. Therefore, there would be no spring-in except spring-in due to thermal contraction when the part was released from the tool. This is presented in the Figure 1.7. Both the analysis and experimental results showed that spring-in angle was decreased when the part thickness increased. Moreover, they observed that the ratio of arc length to the part thickness and the ratio of in-plane modulus to rubbery interlaminar shear modulus affected the spring-in angle. When the arc length was short compared to the part thickness, shearing could occur and therefore spring-in angle decreased. The increase in the ratio of in-plane modulus to rubbery interlaminar shear modulus reduces the spring-in. In the rubbery state, shear modulus of the resin is low as compared to the in-plane modulus of the composite. When cure shrinkage starts, the low shear modulus allows the fibers to maintain the same arc length by sliding in the corner.

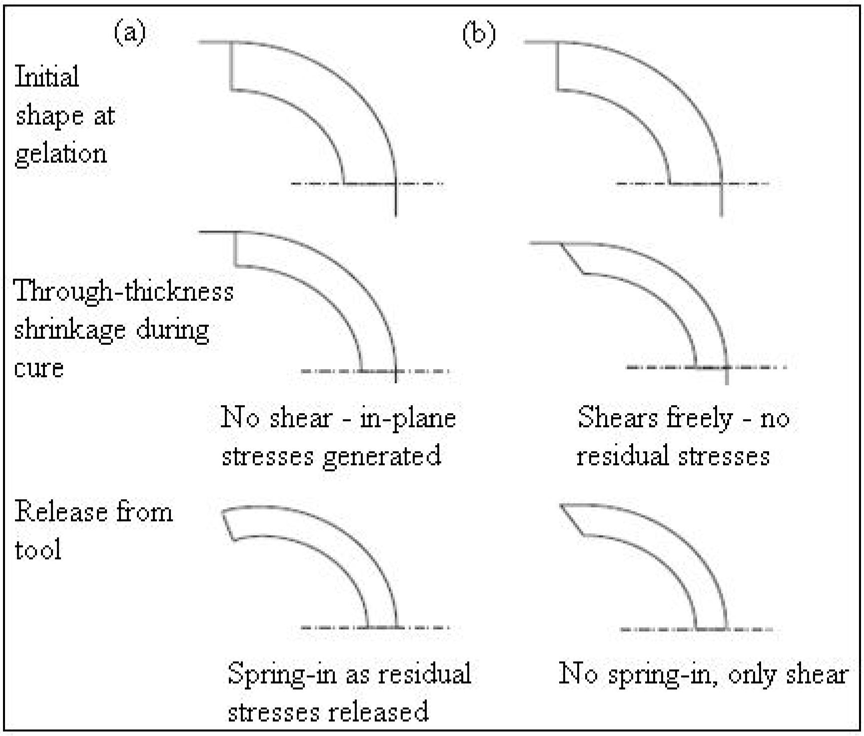

Figure 1.7. The effect of through-thickness contraction on spring-in angle. a) Stiff in shear b) No restriction in shear [17]

In the study of Ferlund and Albert [3], they indicated that part thickness had an effect on spring-in. They performed their experiments with release agent and release agent + FEP on the tool. They found that thin parts gave greater spring-in than corresponding thick parts. According to another research, the thicker parts were more robust compared to the thinner ones [13, 18].

1.2.1.5. Ply-Orientation. Experimental and numerical work carried out by Darrow and Smith [18], tested the influence of fiber orientation on spring-in. They compared the [0] and [+45/-45] laminates. The result of this study showed that the biased laminate [+45/-45] had greater spring-in although by only small amount (< 0.1^{o}).

Radford and Rennick [5] concluded that ply-orientation affected both thermoelastic and non-thermoelastic components. All samples they used had 8 plies and a 6.4 mm corner radius. The $[0]_8$ and $[0/+30/0/-30]_s$ specimens gave much lover thermoelastic response because they had large in-plane thermal expansion coefficient in 90^{o} direction, which is close to the through thickness value of thermal expansion coefficient. The highest value of spring-in was observed in $[90/0/90/0]_S$. Non-thermoelastic response was also high for all specimens. It was raging from nearly 0.64 to 1.12 degrees.

Ferlund and Albert [3] studied the effect of design and processing parameters on spring-in. One of the design parameter was part lay-up in their work. They indicated that quasi-isotropic laminates gave greater spring-in than unidirectional laminates (0^o). Another study of Ferlund *et al* [8] observed similar results. The quasi-isotropic specimens (16 plies) had the greatest spring-in, on the other hand cross-ply and unidirectional samples were slightly smaller. Moreover, the numerical and experimental results were close to each other.

According the study of Ersoy *et al* [19], predicted and measured spring-in values for unidirectional laminates was smaller than the values for cross-ply laminates, and the difference comes from the non-thermoelasic component of spring-in.

The effect of ply-orientation in the work of Garstka [1] was a bit different from the Ferlund *et al* [8] because in the study of Garstka, cross-ply laminates gave more spring-in than the quasi-isotropic ones.

1.2.1.6. Corner Radius. The effect of corner radius on spring has been unclear. There is a disagreement between studies in the literature. Radford and Rennick [5] have concluded that corner radius had an effect on spring-in in their studies. Spring-in is smaller for larger radius. According to their explanation for reason of this observations, for larger corner radius local corner thinning would be less as compared to small radii.

In the studies of Darrow and Smith [18], the results showed that the contribution of corner radius was small ($< 0.2^o$) and smaller corner radius lead to smaller spring-in.

Huang and Yang [10] and Benzie [13] have indicated that the spring-in was independent of the corner radius of the mold. Moreover, Garstka [1], concluded that there was no significant effect of corner radius on spring-in.

1.2.1.7. Flange Length. The effect of flange length on the thermoelastic response of spring-in was investigated by Garstka [1]. He did not observe any difference between the specimens processed different flange lengths.

Experimental work carried by Ferlund and Albert [3], demonstrated that samples with greater flange length gave more spring-in compared to shorter ones but in this work measured spring-in consists of both the thermoelastic and non-thermoelastic component.

1.2.1.8. Part Shape. Ferlund and Albert [3] performed some experiments to investigate the effect of part shape on spring-in. The results of the experiments indicated that the effect of part shape was so small whereas another study of Ferlund *et al* [8] found that C-shaped samples had nearly % 30 greater spring-in than L-shaped samples.

Poursartip and Hubert [20] investigated the variation of the laminate thickness and local fiber volume fraction by using male (convex) and female (concave) tools. They observed that shear flow led to high strains through thickness of the laminate for a [90^o] lay-up at the corner, which creates corner thinning for a male tool and corner thickening for a female tool. Therefore, this thickness gradient had an effect on spring-in.

1.2.1.9. Fiber Volume Fraction Gradients and Consolidation. The contribution of fiber volume fraction gradient to the spring-in was examined by Darrow and Smith [18]. The effect of the fiber volume fraction gradient was obtained by using a bleeder cloth at the bag side. After the process, resin rich region developed at the mold side and the fiber rich region at the bag surface, however this contribution was only important for thin parts. It was also indicated that this effect could be weakened by eliminating resin-absorbing materials in the process.

In their study Hubert and Poursartip [20] performed experimental investigation on the compaction of the angled composite laminates by using two types of material, low viscosity AS4/3501-6 and high viscosity AS4-8552. The laminates of low viscosity resin gave more resin loss compared to the high viscosity resin. The total compaction strain for low viscosity resin was caused by percolation flow under bleed condition but for high viscosity resin, the total compaction strain resulted from percolation and compaction caused by the collapse of voids. The laminate of low viscosity resin was analyzed to determine the fiber volume fraction gradients for processes with or without bleeder. The data obtained from the experiments indicated that fiber volume fraction was low at the tool side and high at the bag side in the bleed condition. The fiber volume fraction measurements through the thickness and in the longitudinal direction showed that net percolation flow from the tool to bleeder occurs. There was a small amount of internal percolation flow from the corner to the flat section of the part in the no-bleed condition.

1.2.1.10. Effect of Prepreg Material. Effect of prepreg material on spring-in was investigated by Ferlund *et al* [8]. Their prepreg materials were T800H/3900-2 and AS4/8552. Results of experimental work indicated that T800H/3900-2 gave less spring-in than AS4/8552, on the other hand predicted spring-in was higher T800H/3900-2.

According to experimental result of Benzie [13], the laminates of low viscosity resin behaved less erratic and produced better mean and variability results.

1.2.2. Numerical Predictions

Some computational models related to autoclave processing have been performed to date.

Johnston *et al*. [21] developed a plane strain finite element model which employs a cure hardening, instantaneous linear elastic constitutive model to predict process-induced stress and distortion of composite laminates. They analyzed the effect of thermal expansion, cure shrinkage, temperature gradients, degree of cure, resin flow and mechanical constraints on the deformation of the laminates. The tool-part interaction was modeled by elastic “shear layer”, which performed until the tool is removed. Their predicted and measured spring-in values were correlated for $[0]_{24}$ sequences, however the correlation was bad for $[90]_{24}$.

Ferlund *et al*. [8] used the model (COMPRO) developed by Johnston [21] to investigate the effects of cure cycle, tool surfaces, geometry, and lay-up on the spring-in of curved laminates. COMPRO was a two-dimensional finite element code to model an autoclave process. For the finite element formulation COMPRO used bilinear quadrilateral isoparametric finite elements to mesh the domain. Single layer finite elements having transversly isotropic elastic properties were used to model the tool-part interaction. In their experimental study, they used release ply (FEP). The representations of release ply in the code performed by a soft shear layer, allowing relative motion between the part and the tool during the cure cycle. A tool surface with no FEP was represented by hardening shear layer. COMPRO determined the effect of tool-part interaction, part shape, lay-up, prepreg material, and cure cycle. The main drawback of COMPRO was that it was 2-Dimensional and the properties of the shear layer sould be calibrated. The COMPRO predictions agreed with the measured trends for the effect of lay-up, part geometry, tool surface condition, and cure cycle, however the trend was not similar for the effect of prepreg material.

In their study Svanberg and Holmberg [16, 22, 23] developed a simplified mechanical constitutive model to predict the shape distortions. They assumed that the mechanical behavior of the material is constant within each material phase and there is a step change in the properties at the glass transition temperature. The rubbery properties they used were simply assumed to be about two orders of magnitude smaller than those in the glassy state. They used three different tool-part interaction models in their FE analysis; freestanding, fully constrained, and frictionless contact conditions. The predictions indicated that the contact boundary conditions give closest agreement to the measured spring –in. Then they used their finite element model to predict the spring-in in brackets produced by Resin Transfer Molding. There were no experimental data about the rubbery properties and the tool-part interaction was oversimplified, which were the main drawbacks of their numerical works.

Ersoy [19] developed a three step 2-D finite element model including anisotropy in the thermal expansion coefficient, cure shrinkage, consolidation, and tool-part interaction to predict the process induced stress and deformation. The three step model was representing the viscous, rubbery, and glassy states of the resin. The aim of preferring three step approaches was the complexity of the determining continuous development of material properties during cure schedule. In each step constant material properties were used. Gelation occurring at approximately 30 % degree of conversion, and vitrification occurring at approximately 70 % degree of conversion for the resin, were two main transitions during the curing process. Ersoy used these transitions between the steps of his model. In the first step of the model, before gelation, viscous material properties were used. In the second step, between gelation and vitrification, rubbery material properties were used and in the last step, after vitrification, glassy material properties were used in the model. Frictional contact was preferred between the interface of the tool and part and also between the individual plies. The drawback of this work was that the material properties used in viscous state was taken as the 1/10 of corresponding value in the rubbery state with is an assumption with no experimental evidence. The material properties can be used after finding the real values. The tool material implemented in the code did not deform. Elastic modulus of the tool was 148×10^{12} MPa.

The present study adopts the three-step model developed by Ersoy [19] and compares the predictions with measured spring-in angles of L shaped parts. The effect of tool-part interaction, cure shrinkage, consolidation, and material anisotropy on spring-in and warpage was examined.

2. NUMERICAL WORK

In the production of composite materials, especially continuous-fiber-reinforced thermoset laminates, observations indicate that the final shape of the composite parts is not same as the mold shape after the process, which in turn cause problems during and after the assembly of parts due to poor contact between mating surfaces.

In the applications a trial and error approach is preferred to solve the problems but this method is very expensive and time consuming in the production of big and complex components; therefore numerical studies are required.

2.1. Finite Element Analysis of Spring-In

2.1.1. Finite Element Model Development

The observations indicate that, during an actual autoclave process with the MRCC, the thermosetting resin is to be found in three forms: viscous, rubbery, and glassy state [24].

In the first step, the resin is in the viscous (liquid) state. The composite cannot sustain any mechanical stress in the transverse direction, whereas it can sustain some fiber stresses. However, the shear modulus of the resin is practically zero, because of fiber friction shear stresses arising from tool interaction or interply shear can be transferred in the through-thickness direction [23]. Also, consolidation takes place as the voids are suppressed, expelled from the composite, and extra resin bleeds out.

In the second step, the resin is in the rubbery state and the elastic modulus is the rubbery modulus of a few MPa. Due to cross-linking reactions, cure shrinkage takes place during the curing of thermosetting resin, which results in contraction in the through thickness direction. Also, the autocalve pressure is applied.

Finally, in the third step, the resin vitrifies and transforms to the glassy state and the resin modulus increases to a magnitude of a few GPa. The deformations occurring in rubbery state are fixed in and the part is allowed to deform freely as it cools down to room temperature by removing the boundary conditions.

The model implemented in this study assumes that the mechanical properties are assumed to be constant within each material phase; viscous, rubbery, glassy, and the mechanical properties of a single lamina are transversely isotropic.

In this study, viscous state is represented in Step-1, rubbery state in Step-2 and glassy state in Step-3 respectively. Although the FEM is executed as a 3-Step Model, the material properties of the resin used in Step-1 and Step-2 are the same because there is no data regarding to the viscous properties of the resin. However, since it is mentioned above that significant fiber stresses develop between tool and part interface in the viscous state, this state is included into the model as first state. Initial temperature of the part and tool are 331 ^{o}C and 20 ^{o}C respectively. The reason of high initial temperature of the part is to obtain 0.5 % cure shrinkage in the rubbery state as the part cools from 331 ^{o}C to 180 ^{o}C. In Step-1 and Step-2, an autoclave pressure of 0.689 MPa is applied on the bag surface of the part. In Step-3, the applied pressure is removed and part is separated from the tool and spring-in and warpage develops. The applied temperature and pressure in all three steps can be seen in Table 2.1.

Table 2.1. The applied temperature and pressure in the steps.

		Temperature		Pressure
		Part	Tool	
	Initial	331 ^{o}C	20 ^{o}C	-
Viscous	Step-1	331 ^{o}C	165 ^{o}C	0.689 MPa
Rubbery	Step-2	180 ^{o}C	180 ^{o}C	0.689 MPa
Glassy	Step-3	20 ^{o}C	20 ^{o}C	-

2.1.2. Material Constitutive Model

The analysis is performed for AS4/8552 composite system and the thermoelastic properties of the resin in the rubbery and glassy states are obtained by using Finite Element Based Micromechanics (FEBM), which models the composite as a hexagonal array of perfectly aligned fibers in a matrix of resin [24]. Calculated rubbery and glassy state properties of the resin are listed in Table 2.2. The tool material is steel with an elastic modulus of 200 GPa and thermal expansion coefficient of 12.6x10^{-6} $^{o}C^{-1}$.

The material coordinate system is represented in Figure 2.1, where the fiber direction is the *1*-direction, the transverse direction is the *2*-direction, and the through-thickness direction is the *3*-direction. The constitutive relation for the composite in the rubbery and glassy state can be expressed as:

$$\begin{Bmatrix} \varepsilon_{11} \\ \varepsilon_{22} \\ \varepsilon_{33} \\ \gamma_{12} \\ \gamma_{13} \\ \gamma_{23} \end{Bmatrix} = \begin{bmatrix} 1/E_{11} & -\nu_{12}/E_{11} & -\nu_{13}/E_{11} & 0 & 0 & 0 \\ -\nu_{12}/E_{22} & 1/E_{22} & -\nu_{23}/E_{22} & 0 & 0 & 0 \\ -\nu_{13}/E_{33} & -\nu_{23}/E_{33} & 1/E_{33} & 0 & 0 & 0 \\ 0 & 0 & 0 & 1/G_{12} & 0 & 0 \\ 0 & 0 & 0 & 0 & 1/G_{13} & 0 \\ 0 & 0 & 0 & 0 & 0 & 1/G_{23} \end{bmatrix} \begin{Bmatrix} \sigma_{11} \\ \sigma_{22} \\ \sigma_{33} \\ \tau_{12} \\ \tau_{13} \\ \tau_{23} \end{Bmatrix} \tag{2.1}$$

where for a transversely isotropic composite, $\nu_{12} = \nu_{13}$ $, E_{22} = E_{33}, G_{12} = G_{13}$, and $G_{23} = E_{22}/2(1+\nu_{23})$.

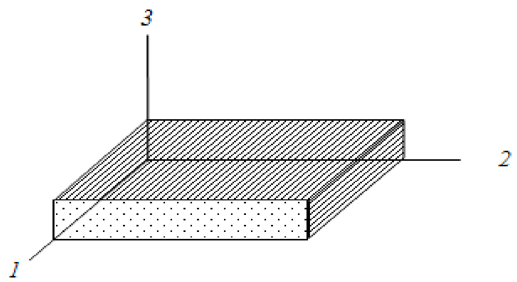

Figure 2.1. The fiber, transverse, and through-the-thickness directions.

Table 2.2. Composite material properties in the rubbery and glassy states in modeling.

Property	Unit	Rubbery	Glassy
E_{11}	MPa	132200	135000
$E_{22} = E_{33}$	MPa	165	9500
$G_{12} = G_{13}$	MPa	44.3	4900
G_{23}	MPa	41.6	4900
$\nu_{12} = \nu_{13}$	-	0.346	0.3
ν_{23}	-	0.982	0.45
α_{11}	με/°C	-	0
$\alpha_{22} = \alpha_{33}$	με/°C	-	32.6
ε_{11}^{cure}	%	0	-
$\varepsilon_{22}^{cure} = \varepsilon_{33}^{cure}$	%	0.48	-

2.1.3. Meshing and Boundary Conditions

The L-section-composite parts of 100 mm arm length and 15-25 mm corner radius are modeled in female steel tool, in Figure 2.2. Only the half of the part is modeled by taking advantage of the symmetry condition.

In the first step, compaction and tool interaction occur up to gel point where T= 165 °C. Initial temperature of the part and tool are 331 °C and 20 °C respectively. In the second step, cure shrinkage and tool-part interaction occur. The reason of high initial temperature of the part is to obtain 0.5 % cure shrinkage in the rubbery state as the part cools from 331 °C to 180 °C. Generalized plane strain condition is applied, and only rotations are constrained in this step. Meshing and boundary condition are seen in Figure 2.2 (a). Symmetry boundary condition is used to reduce the calculation time of the model. In the third step, state, in-plane stiffness of the material increases and the autoclave pressure is removed. In the absence of any external forces, the plane stress condition is assumed to be valid during the third step of the analysis. The use of generalized plane strain elements enables the transition from the plane strain condition to plane stress condition by removing the translation restraint imposed on the references nodes. Meshing and boundary condition of third step is shown in Figure 2.2 (b).

(a)

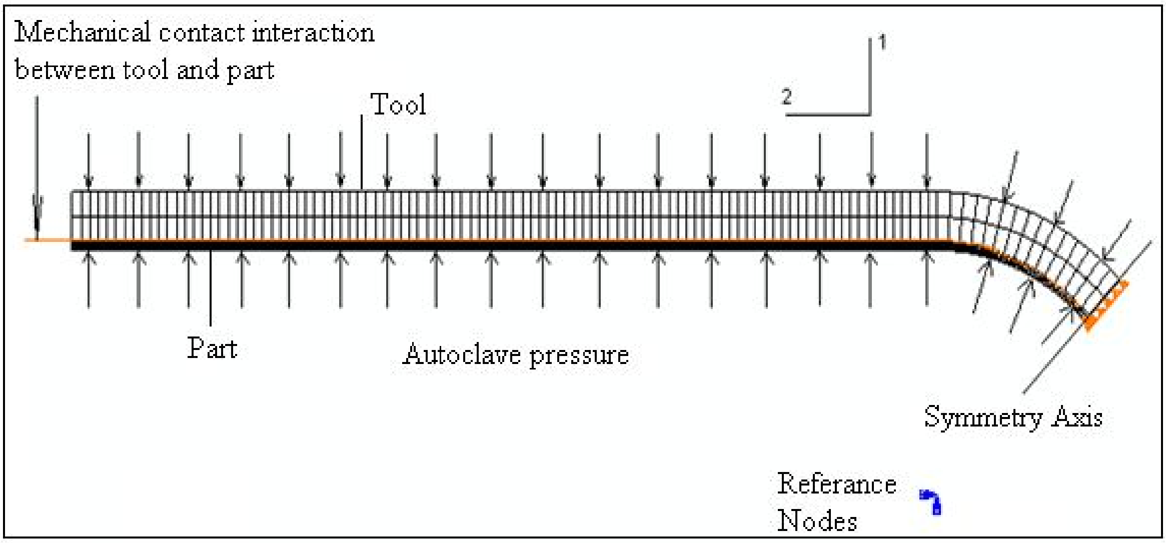

(b)

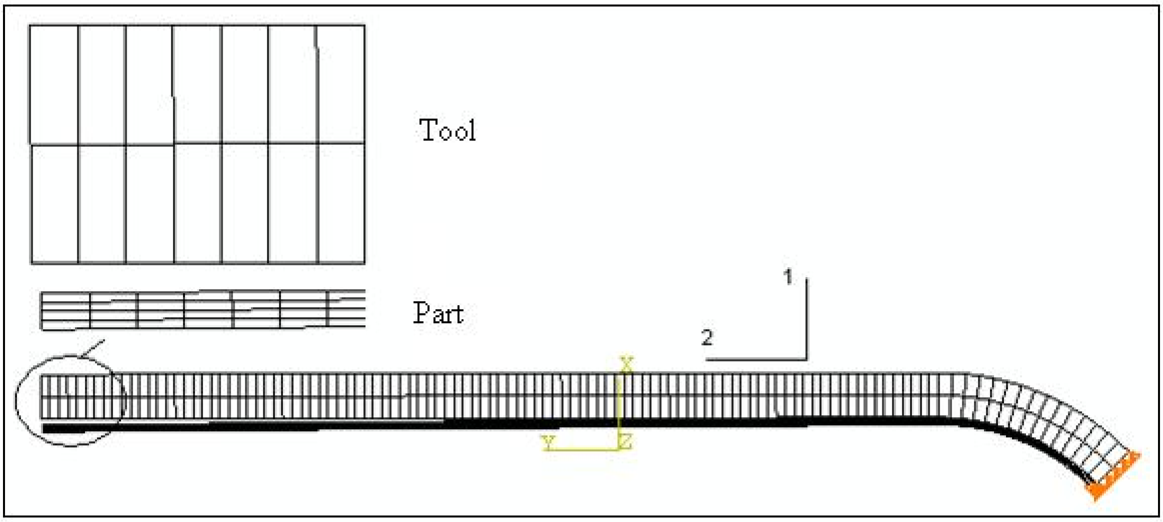

Figure 2.2. The finite element mesh and boundary condition for the L-shaped sections in Step-1 (a) and Step-3 (b).

The elements used in the code are 8-node biquadratic quadrilateral generalized plane strain elements with reduced integration. The name of the element in ABAQUS is CPEG8R [25]. The generalized plane strain theory used in ABAQUS assumes that the model lies between two planes that can move with respect to each other. It is assumed that the deformation of the model is independent of position with respect to this direction, in turn, the relative motion of the two planes results in a direct strain in the direction perpendicular to the plane of the model only. The defined generalized plane strain elements have an extra node with 3 degrees of freedom; an out of plane translation and two rotations. Restraining this node gives a plane strain condition whereas; releasing the node gives plane stress condition. In the model, two reference nodes are defined for both the tool and the part in all the steps for unidirectional parts. These reference nodes are restrained for rotation so that the two bounding planes displace with respect to each other but do not rotate freely, which allows the thermal expansion effect of the tool perpendicular to the plane of the model to be considered, and such restraint prevents the spread of the part from the tool under pressure in the first and second steps. In cross-ply parts, only one reference node is defined. In Step-3, the part is removed from the tool, so that the part is now in plane stress condition; the absence of external forces in Step-3 validates the plane stress condition.

Tool-part interaction is modeled by using ABAQUS mechanical contact interaction modeling capabilities. In the model, contact surfaces are defined for interactions, using ABAQUS option *SURFACE, and then these surfaces are matched by using the option *CONTACT PAIR. The characteristic of the contacting surfaces are defined by using the option *SURFACE BEHAVIOUR.

Interaction normal to the surface is the default "hard" contact relationship, which allows no penetration of the slave nodes into the master surface and no transfer of tensile stress across the interface. Interaction tangential to the surface is modeled by the classical isotropic Coulomb friction model. In the Coulomb friction model, the interfacial shear stress is proportional to the contact pressure up to a limiting sliding stress, and the constant of proportionality is the friction coefficient, μ and the limiting stress is τ_{max} as shown in Figure 2.3.

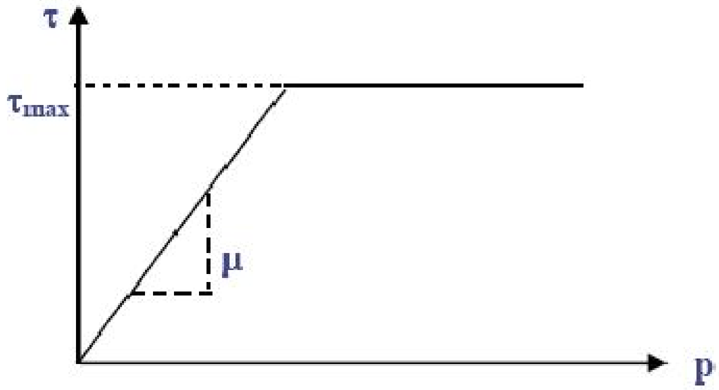

Figure 2.3. Interface friction characteristics

In the model, friction coefficient and maximum shear stress are 0.3 and 0.17 MPa respectively [1]. Maximum shear stress value was measured experimentally by Garstka for single plies cured in a flat aluminum tool, and the maximum shear stress was used here for steel tool, since there was no data available for limiting sliding stress between prepreg and steel tool. For the friction coefficient, 0.5-0.8 was used in the literature for polymer resin and polished steel tool. The tool was covered with release film so that the fiction coefficient was preferred to be 0.3.

3. EXPERIMENTAL WORK

An experimental approach is presented in this chapter which includes the manufacturing of the autoclave mold, the production of the L-shaped composite specimens and the data collection process of the produced specimens.

3.1. Manufacturing of the Mold

The autoclave equipment consists of a U shaped steel tooling which was machined from a solid block. The material of the solid block was IMPAX P20 Hot Work tool steel. The width of the C shaped tool is 200 mm, the flange length is 170 mm and the thickness of the tool is 15 mm. The U-shaped tool had two corner radii of 25 and 15 mm. Also, the tool surface is mirror polished condition. The 3-D geometry of the tool is shown in Figure 3.1.

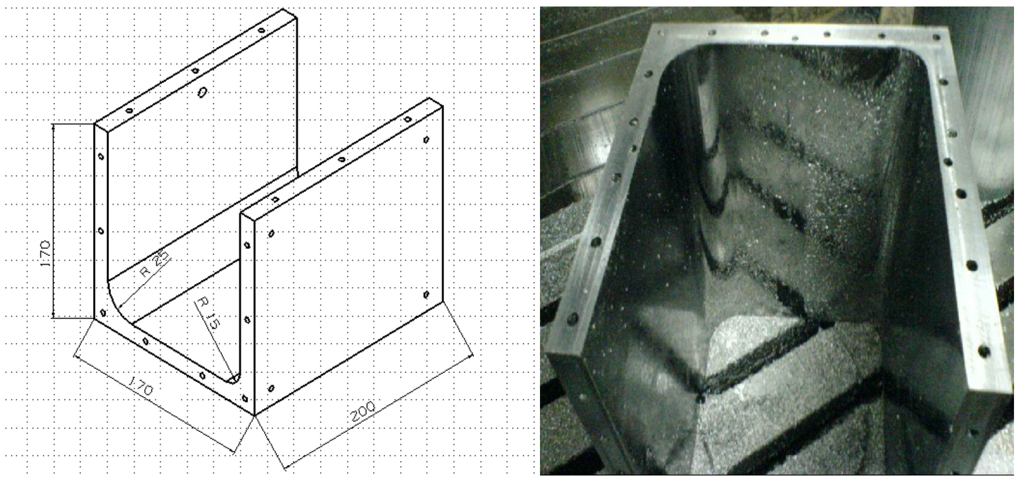

Figure 3.1. 3-D drawing of the tooling and the manufacturing of the tooling

Heat was applied around the U shaped tool with plate heaters and pressure was applied through the vacuum port and the compression port which is shown in Figure 3.2.

The temperature was controlled with a three-channel PID controller. The uniformity of the temperature around the surface of the U shaped tool was be checked by a data acquisition with 8 thermocouple input ports.

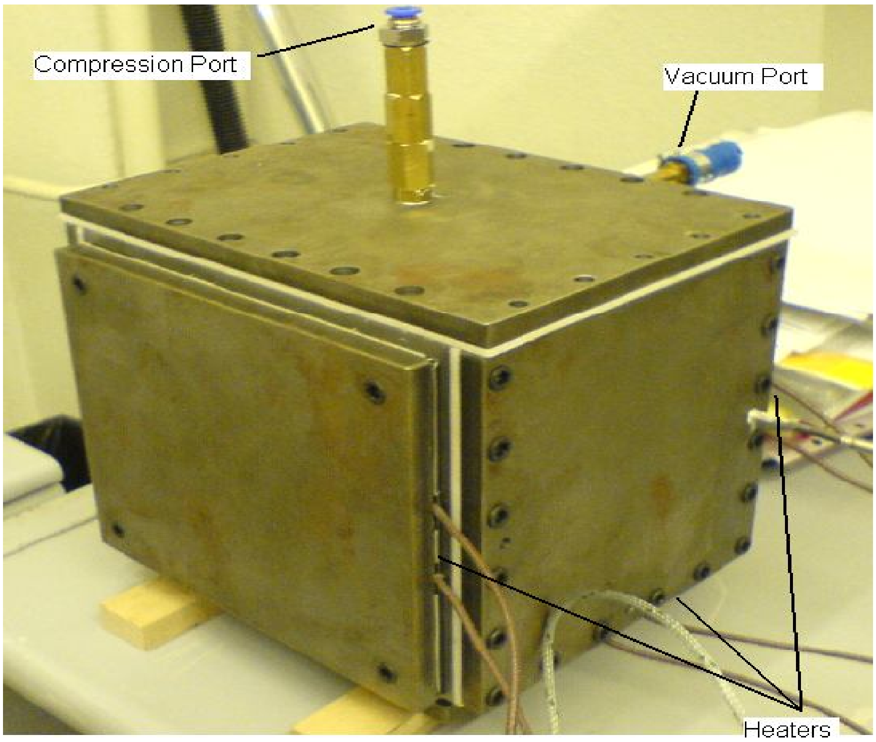

Figure 3.2. Representation of the mold.

3.2. The Production of the L-shaped Composite Specimens

3.2.1. Materials Used

The material used was AS4/8552 unidirectional tape manufactured by the HEXCEL Company. Physical properties of the prepregs are given in the Table 3.1. The thickness of a single ply is 0.184 mm.

Table 3.1. Physical properties of AS4/8552 [26]

	Units	AS4
Fibre Density	g/cm^3	1.79
Resin Density	g/cm^3	1.30
Nominal Cured Ply Thickness 8552/35%/134	mm	0.130
Nominal Fibre Volume	%	57.42
Nominal Laminate Density	g/cm^3	1.58

3.2.2. Applied Cure Cycle

The nominal cure cycle was applied in this work for the AS4/8552 composite system, which is recommended by the manufacturer, is shown in Figure 3.3. The manufacturer recommended cure cycle (MRCC) includes five steps. In the first step, the part is heated-up to 120 ^{o}C at 2 ^{o}C / min. Then in the second step, it is held 60 minutes at 120 ^{o}C. In the third one, it heated-up from 120 ^{o}C to 180 ^{o}C at 2 ^{o}C / min. Then, the part is held 120 minutes at 180 ^{o} C. Finally, the part is left to cool down to room temperature before the part is removed from the mold. Pressure (0.689 MPa) is applied from beginning to end of the process and vacuum (0.1 MPa) is used up to middle of the second step.

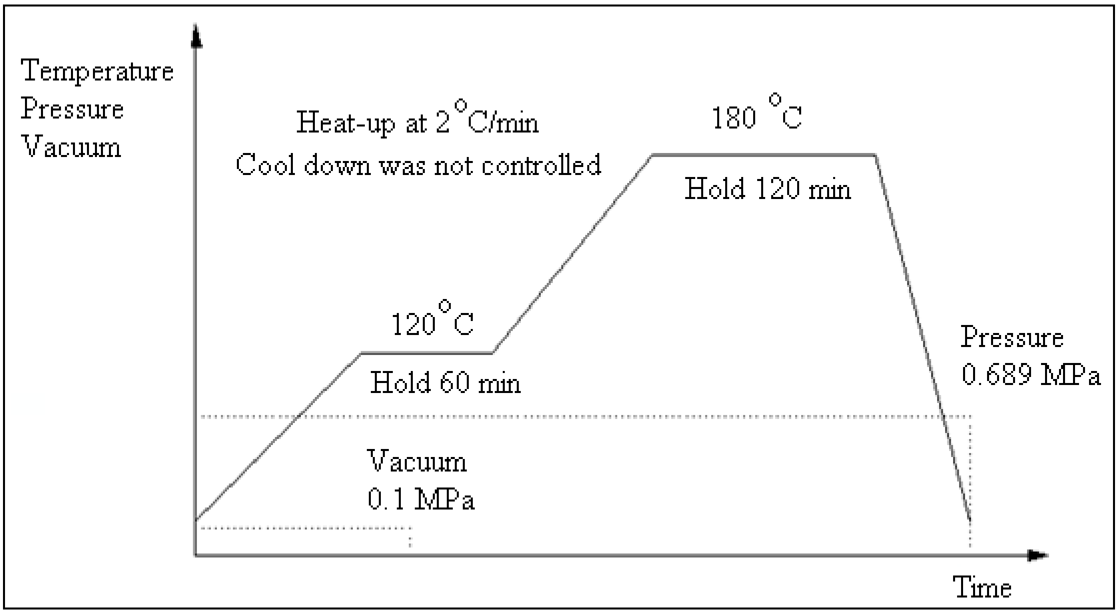

Figure 3.3. Cure Cycle for the AS4/8552 composite system

3.2.3. Specimen Preparation

All specimens in this work were fabricated by hand cutting and hand lay-up of the carbon-epoxy prepreg material, followed by curing. The schematic drawing of the process is shown in Figure 3.4.

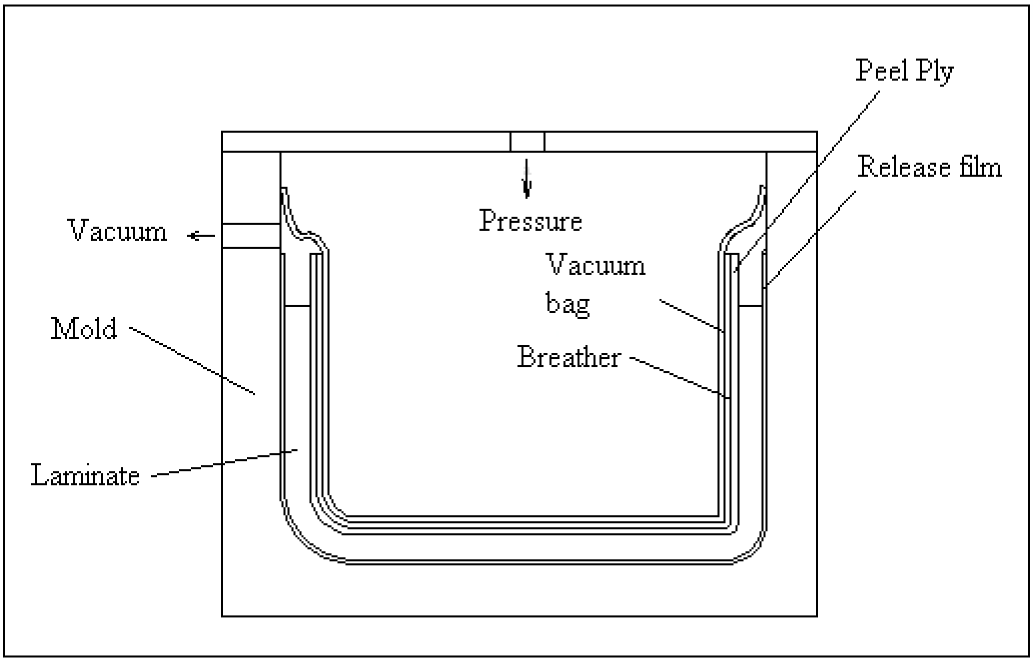

Figure 3.4. The schematic drawing of the process

Before starting the process, the tool surfaces were cleaned with acetone to remove traces of oil and dirt. Teflon coated glass fabric release film of 0.12 mm thick then applied over the entire surface, which allows for easy removal of cured parts and good slip of prepregs from the tool. Each ply of the prepreg was carefully laid-up on only one side of the mold shown in Figure 3.5. A vacuum of approximately 0.1 Mpa was applied for every six plies to consolidate the samples, remove entrapped air and minimize the possible effect of corner bridging.

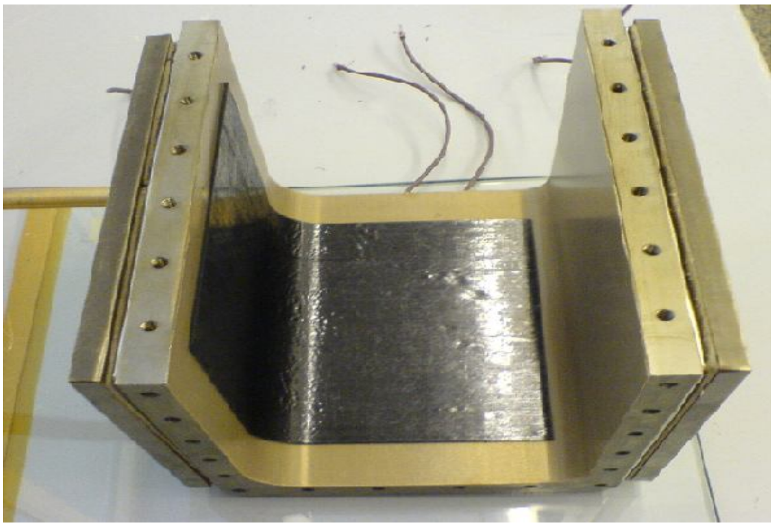

Figure 3.5. Prepregs laid-up on the mold.

The laid-up prepregs were then covered with peel ply. It can be seen in Figure 3.6. Peel plies are woven fabrics that are generally applied as the last material in the composite laminate sequence and designed to leave a textured surface on the fabricated composite parts.

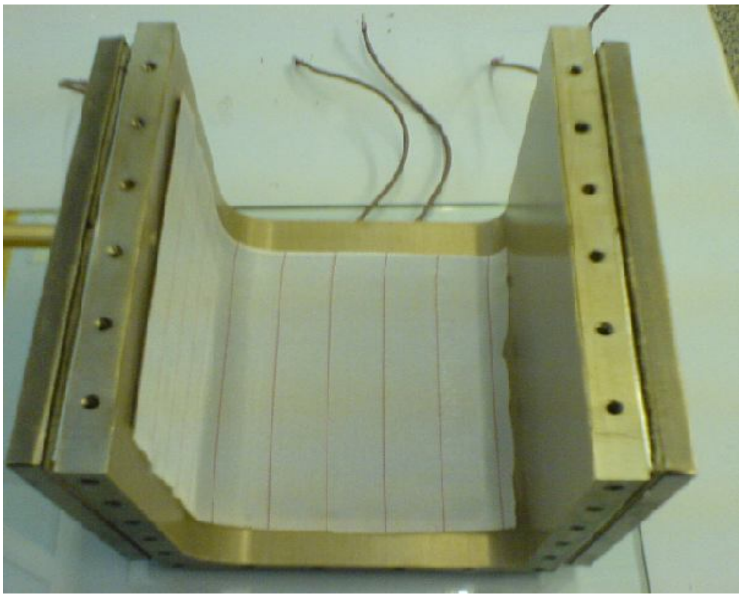

Figure 3.6. Peel ply was applied on the prepregs.

On the peel ply, a breather fabric was laid-up to perform two functions. The first, as the name suggests, is to allow the vacuum stack to 'breathe'. This breathing function ensures that the air sealed under the vacuum bag can be easily extracted. It also provides a path for the flow of any entrapped air, or volatiles, from within the laminate during the cure cycle. The second function is to absorb any excess resin that is bled from the laminate. In Figure 3.7 a breather fabric is shown.

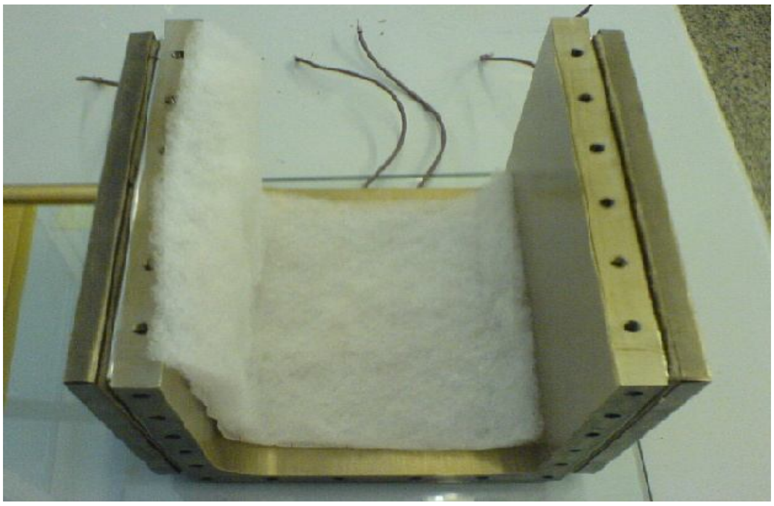

Figure 3.7. A breather fabric was applied on the peel ply.

In the other step, a vacuum bag and a sealant tape were applied to seal the whole composite laminate. It was represented in Figure 3.8

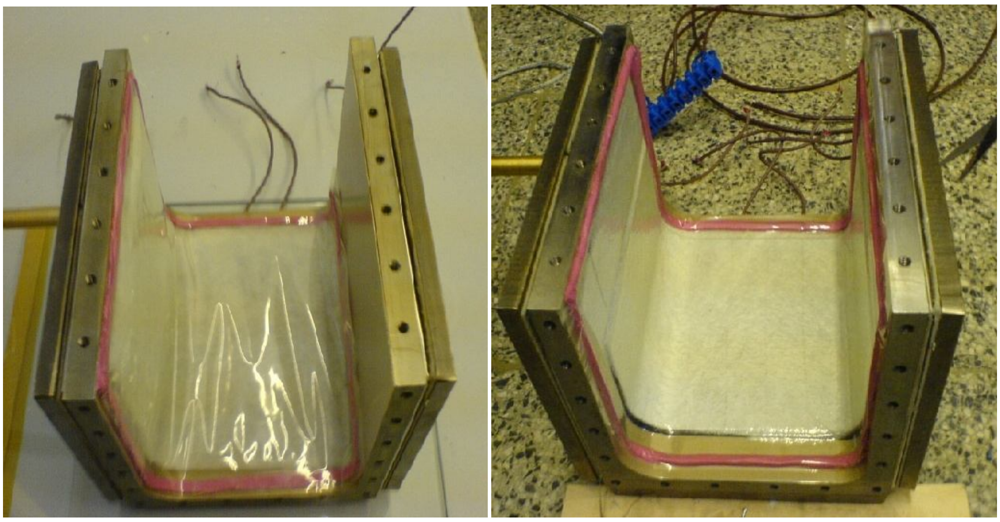

Figure 3.8. A vacuum bag covered all the items.

Finally, the plates of the mold were screwed onto the sides of the mold and then the MRCC process was started, Figure 3.9.

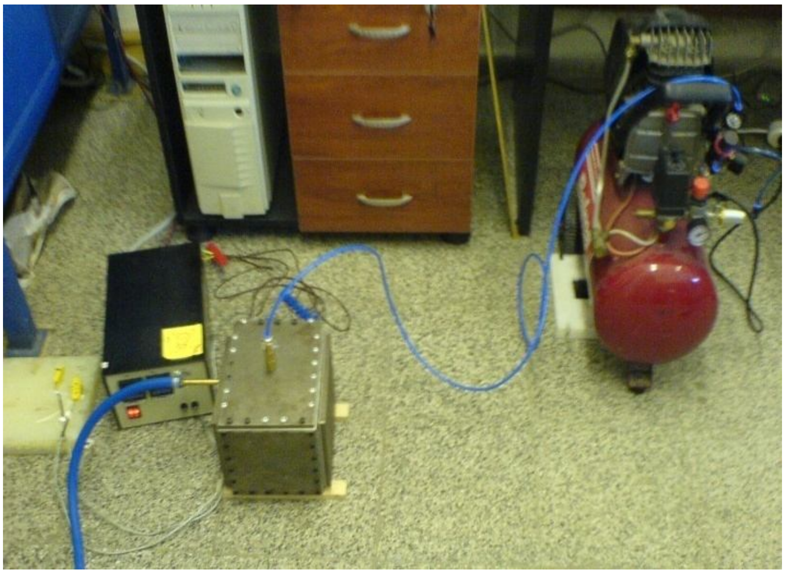

Figure 3.9. The processes was started to cure the prepregs

After processing, the mold was left to cool down to ambient temperature before the composite part was debagged and removed from the mold. Then the produced part removed from the tool, as shown in Figure 3.10.

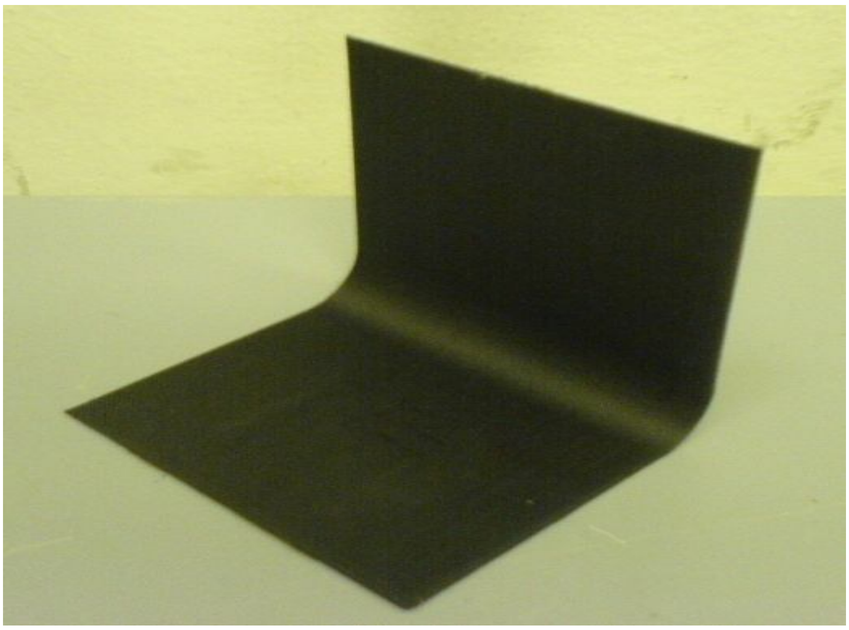

Figure 3.10. L shaped composite part was produced.

3.3. Measurement of Spring-in Angle

The geometry of the produced samples was evaluated by using a high precision 3-D coordinate measuring machine. The samples were fixed to the plate using an epoxy adhesive, as shown in Figure 3.11. In this measurement technique, one should locate the sample carefully because when the probe touches the sample, the sample may deflect, especially for thinner samples.

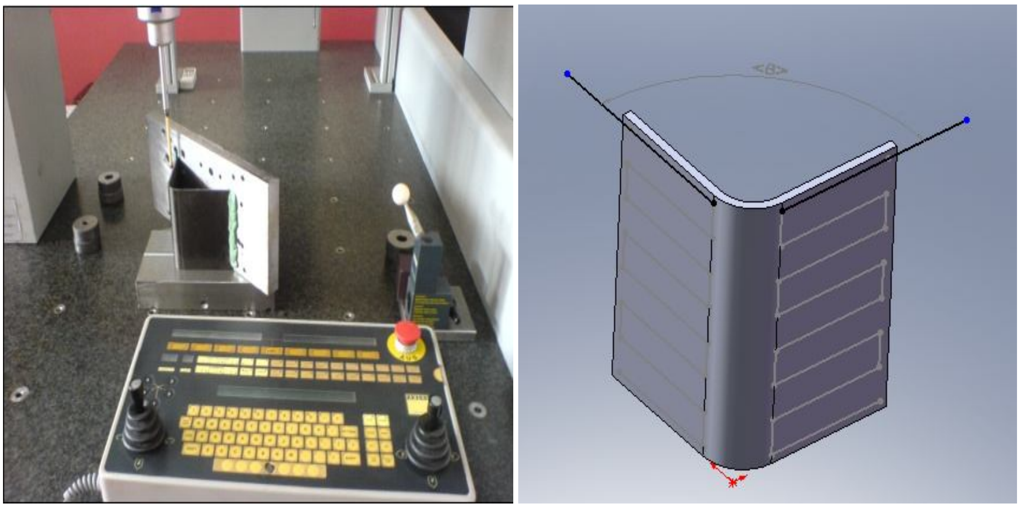

Figure 3.11. 3-D Coordinate measurements of the L-shaped samples

The location of 12 points along the profile was recorded to evaluate the spring-in angle and warpage of the flat arms. The angle between the arms (ß) of the samples was determined by taking the measurements of two points on each side of a corner, as shown in Figure 3.12. The careful observation also showed that the arms of the samples warped concave up from the tool. To evaluate this warpage, the measurements of several points also were taken from the arms of the parts.

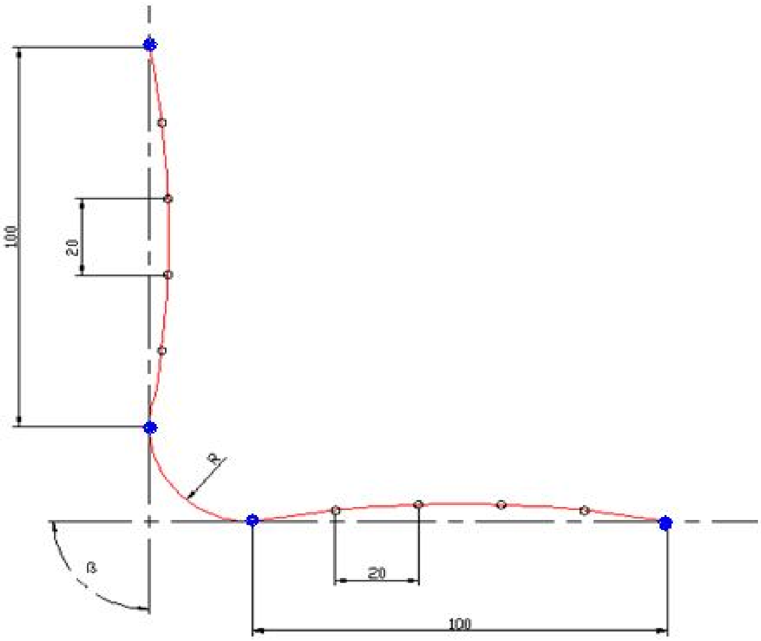

Figure 3.12. The profile of the composite samples

3.4. Specimen Preparation and Optical Analysis Procedures for the Characterization of Fiber Volume Fraction Gradient

The classical way for evaluating the fiber volume fraction of a polymer-matrix composite is acid digestion method. Through this method, fibers detach from the polymer matrix by the digestion of a polymer-matrix using an acid which does not damage the fibers. After digestion, the remaining fibers are washed, dried and then weighed. Knowing the initial weight of the composite sample and the densities of the fiber and resin, the volume fraction of both the fiber and matrix in the original laminate may be determined. This method is not suitable for determining through the thickness fiber volume fraction gradients, it provide only the average fiber volume fraction of the sample. Ply by ply fiber volume fraction differences are not determined by this method. [27]

To obtain the localized fiber volume fraction of the samples, optical microscopy-based image analysis techniques can be preferred. For these techniques, digital cross-section photomicrographs of the sample are required. Thus, samples should be polished using standard metallographic techniques and then their digital images should be recorded at magnifications between 100x and 2500x. The recorded images are 'gray level' images, so they should be converted into binary images (black and white) by segmenting procedures. When segmenting, all pixels within the recorded image with a gray level higher than the chosen threshold value are made white, on the other hand pixels with a grey level lower than the chosen threshold value are made black, in Figure 3.13 [28]. The purpose of the creating this binary image for constituent content determination is to separate the fibers (white) from the matrix (black). After segmenting, digital image analysis techniques (areal method and the fiber counting method) are performed to analyze the resulting binary image to evaluate the fiber and resin volume fractions. [27]

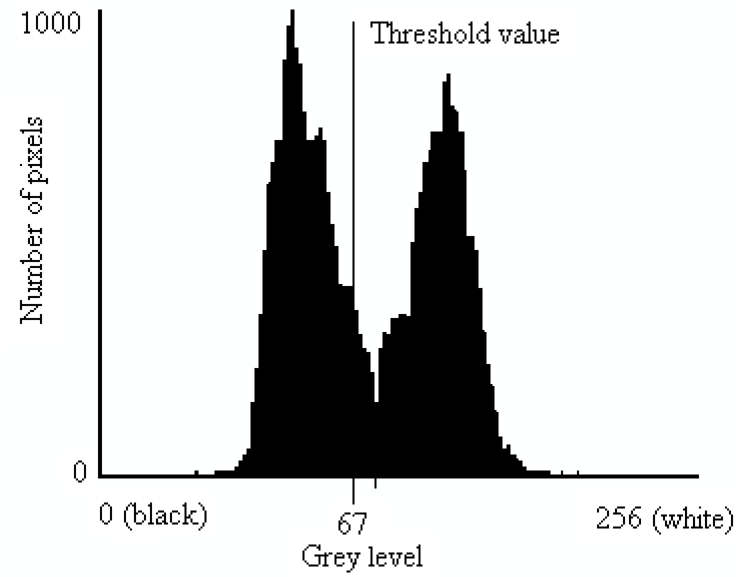

Figure 3.13. Histogram of number of pixels versus gray level

In the areal method, the number of black and white pixels within the specified region of interest is counted using computational algorithm. The volume fraction of the fiber or the matrix in the selected region is determined by dividing their counted area to the total area of the image. To obtain rational results from this method, the magnification of the image should be high and the contrast between matrix and fiber should be sufficient. Also, the threshold value must be selected properly because it affects the volume fraction values excessively [27, 28].

Fiber counting method includes the processing of binary digital image in which each fiber seems white region in a black background, allowing the software to count the number of fibers within a chosen region. The fiber volume fraction is determined by multiplying the number of fibers by the fiber cross-section area and dividing the resultant fiber area by the total area in the selected region [27, 28].

$$V_f = \frac{\pi r_f^2 N_f}{A_T} \tag{3.1}$$

where V_f is fiber volume fraction, r_f is radii of fibers, N_f is the number of counted fibers and A_T is total area of the image.
In the fiber counting method, a watershed feature separation algorithm may be used to eliminate the touching fibers. For example; two touching fibers represent one fiber when the software is calculating the count of fibers; therefore the number of the fibers may be less from the original ones.

As mentioned before fiber volume fraction gradient has an effect on spring-in. Optical microscopy was performed to determine the fiber volume fractions of corner and the arm of the laminates.

A water-cooled diamond saw was used to cut specimens (10 mm x 10 mm squares) from the corner and the arms of produced unidirectional L-shaped composites. These trimmed sections were then potted in epoxy and polished by standard metallographic procedures. The samples grinded with SiC sandpaper by order of 180-240-400-600-1200 grit sizes. Then the samples polished with Al_2O_3 suspension by order of 3-1-0.05 µm.

From each specimen, digital photomicrographs were captured at 50x magnification using (Nikon ECLIPSE NV 150) microscope, Figure 3.14.

Figure 3.14. Photomicrograph at 50x magnification from the corner of a laminate

All image analysis was then performed using a software program called ‘Image J’. An area of interest from the photomicrograph was first selected. After the region of the image to be analyzed was selected, the gray level bitmap images were converted into a black-and-white or ‘binary’ image using segmenting procedure. In the procedure the threshold value is determined automatically by the software. At this point, the fiber volume fraction was determined using the areal method by counting the number of white (fiber) versus black pixel (matrix) and calculating the fraction of the total pixels corresponding to fiber, as shown in Figure 3.15.

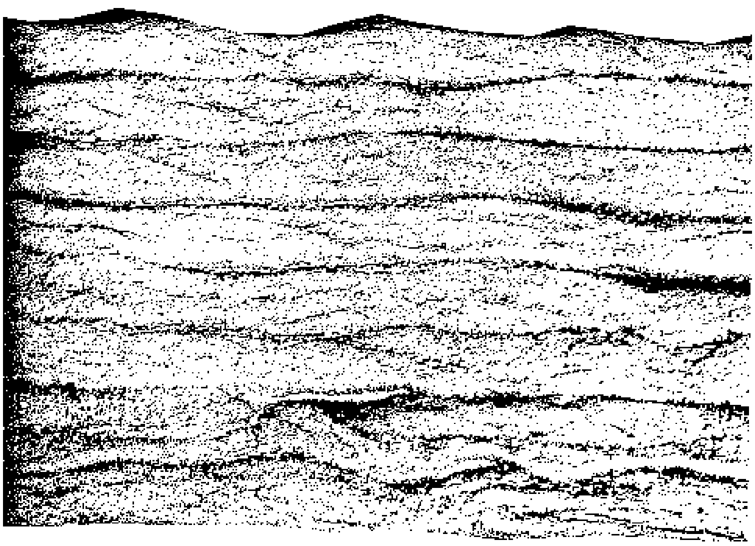

Figure 3.15. Binary image of photomicrograph at 50x

3.4.1. Calculation of Average Fiber Volume Fraction of the Parts after Producing

Nominal fiber volume fraction, nominal laminate density, and the resin density were taken from Table 3.1

The fiber volume fraction is given as

$$V_f = \frac{V^{fibers}}{V^{fibers} + V^{resin}} = 0.5742\ (nominal\ value) \tag{3.2}$$

where V^{fibers} is the volume of the fibers and V^{resin} is the volume of the resin within the composite as the volume of the resin reduces due to resin bleeding, fibre volume fraction increases.

We can find the new rein volume by subtracting the volume of resin that bleeded which can be found by dividing the mass of the bleeded resin by its density.

$$V_f' = \frac{V^{fibers}}{V^{fibers} + V^{resin} - V^{bleed}} \tag{3.3}$$

The uncured stack of prepregs was weighed at first, and after the process is completed the cured part was weighed again. By subtracting the mass of the uncured and cured part, the mass of the absorbed resin could be found. The volume of the uncured prepregs was calculated by dividing the mass to nominal laminate density. Similarly, the volume of the absorbed resin was calculated by dividing the mass of the absorbed resin to its density. The volume of the cured part was calculated by subtracting the volume of the absorbed resin from the uncured volume of the part.

The unknown fiber volume fraction of the manufactured part was calculated by multiplying nominal fiber volume fraction (FVF) with volume of the cured part and then dividing the result to volume of the uncured part. The calculated values are represented in Table 4.2.

4. RESULTS AND DISCUSSION

In this study, effects of stacking sequence, laminate thickness, and corner radius on spring-in were investigated experimentally and numerically. Measured spring-in values and standard deviations for all samples are listed in Table 4.1. Average of eight measurements is taken from the same sample. The effect of various variables is examined in the next section.

Table 4.1. Measured spring-in values for all samples.

Stations	R15-XP-16 Plies	R15-UD-16 Plies	R25-XP-16 Plies	R25-UD-16 Plies
5	1.143	0.753	1.060	0.631
25	1.196	0.861	1.106	0.749
45	1.201	0.896	1.114	0.820
65	1.202	0.907	1.130	0.849
85	1.206	0.904	1.127	0.860
105	1.199	0.873	1.076	0.807
125	1.198	0.827	1.008	0.707
138	1.171	0.751	0.979	0.628
Standard Deviation	0.022	0.064	0.056	0.093
Average Spring-in	1.190	0.846	1.075	0.756
Stations	R25-XP-12 Plies	R25-UD-12 Plies	R15-XP-12 Plies	R15-UD-12 Plies
5	1.070	0.652	1.092	0.642
25	1.126	0.806	1.171	0.780
45	1.187	0.910	1.202	0.846
65	1.218	0.943	1.205	0.855
85	1.224	0.952	1.179	0.848
105	1.176	0.890	1.140	0.814
125	1.101	0.786	1.095	0.755
138	1.020	0.612	1.000	0.602
Standard Deviation	0.073	0.130	0.070	0.097
Average Spring-in	1.140	0.819	1.136	0.768
Stations	R25-UD-8 Plies	R25-XP-8 Plies	R15-XP-8 Plies	R15-UD-8 Plies
5	0.837	0.990	1.203	0.684
25	0.891	1.061	1.240	0.821
45	0.925	1.108	1.250	0.889
65	0.920	1.105	1.252	0.905
85	0.870	1.084	1.125	0.864
105	0.785	0.959	0.994	0.791
125		0.813	0.843	0.704
138			0.712	0.563
Standard Deviation	0.053	0.107	0.207	0.119
Average Spring-in	0.871	1.017	1.077	0.778

Table 4.1. Measured spring-in values for all samples(continue).

Stations	R25-UD-4 Plies	R15-UD-4 Plies		
5	1.046	0.886		
25	1.129	0.909		
45	1.213	0.927		
65	1.259	0.890		
85	1.203	0.837		
105	1.020	0.684		
125	0.624	0.440		
138	0.072			
Standard Deviation	0.406	0.177		
Average Spring-in	0.946	0.796		

4.1. Stacking Sequence Effect

The effect of the laminate sequence on spring-in is represented in Figure 4.1 and Figure 4.2. 8, 12, and 16 plies laminates autoclaved on the steel tool with 15 and 25 mm radius. The results show that cross-ply laminated parts have greater spring-in than unidirectional parts. The findings agree with results from the literature [1, 5, 19]. The through-the thickness CTE and cure shrinkage of the cross-ply parts are greater than the unidirectional parts due to the constraints imposed by fibers in the two in-plane directions in cross-ply parts. For unidirectional parts, predicted spring-in values closely match the measured spring-in values but for the cross-ply parts, the values do not match well. The reason of this may be other non-thermoelastic contributors.

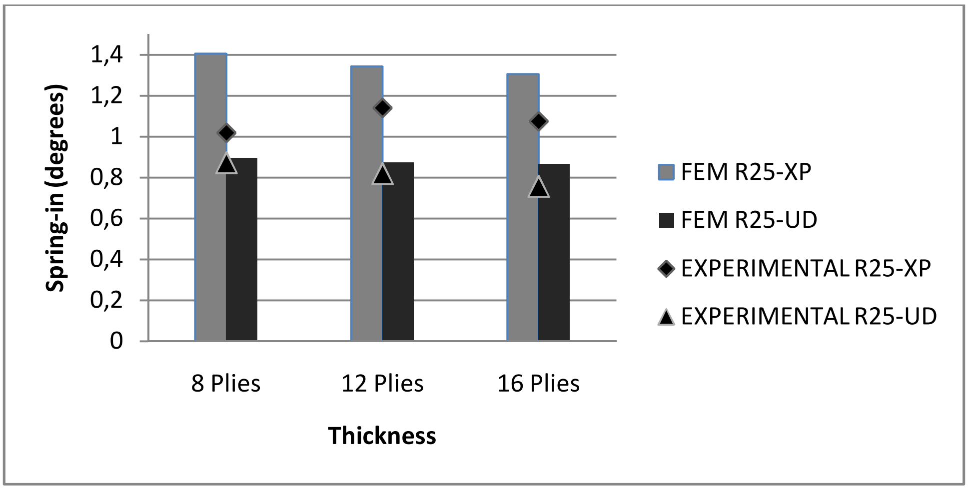

Figure 4.1. Stacking sequence effects on spring-in for 25 mm radius.

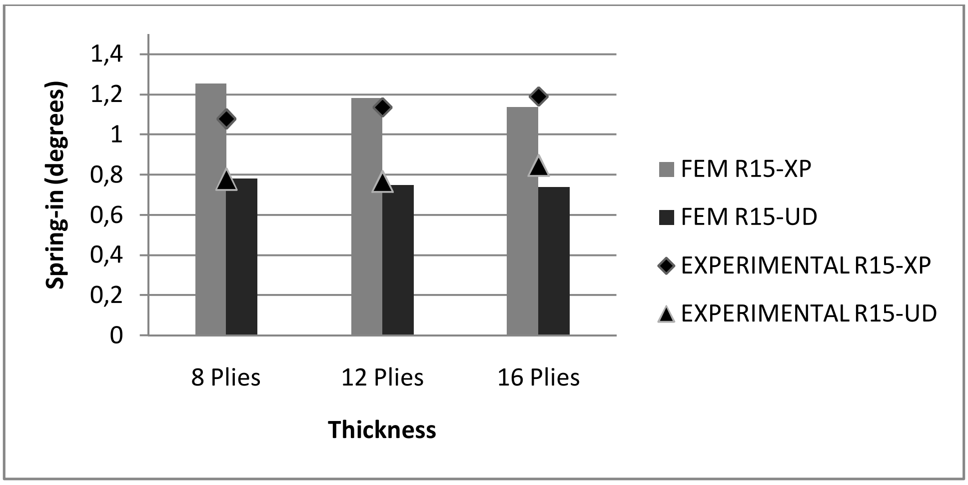

Figure 4.2. Stacking sequence effects on spring-in for 15 mm radius.

4.2. Thickness Effects

Figure 4.3 and Figure 4.4 show the effect of thickness on spring-in for the unidirectional laminates. It is represented that thin parts give higher spring-in as compared to thick parts (except R15-UD-16 plies part) as well as the numerical and experimental spring-in values matched very well. The thicker parts have higher flexural stiffness as compared to the thinner parts, and according to shear-lag theory [17] the slip between plies in viscous and rubbery state decrease spring-in in thick parts so that they have smaller spring-in than thinner parts.

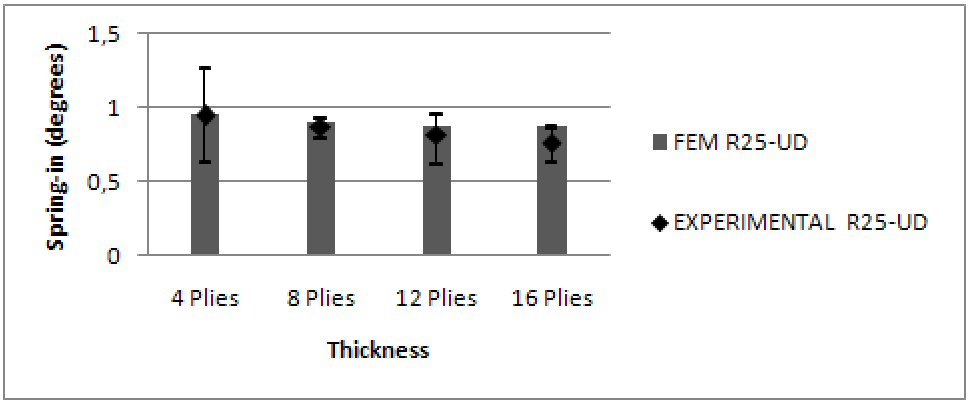

Figure 4.3. Effect of thickness on spring-in for the unidirectional parts with 25 mm radius.

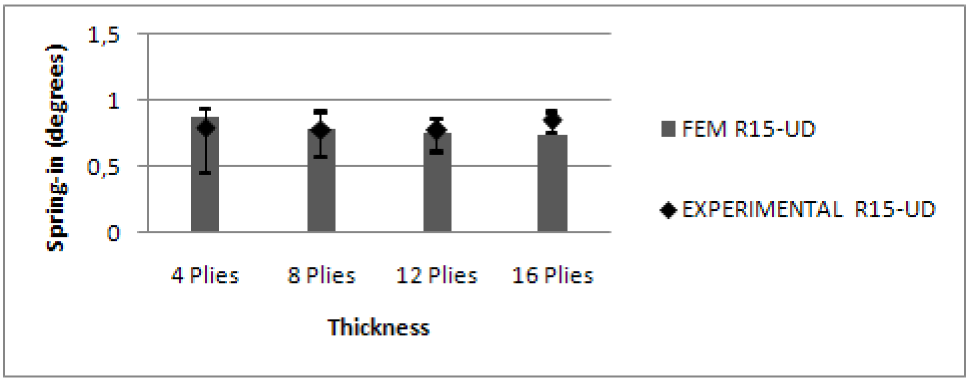

Figure 4.4. Effect of thickness on spring-in for the unidirectional parts with 15 mm radius.

The distortion behavior of the parts is different in cross-ply parts. For the small radius parts, spring-in values increase as the part thickness increases. Although the FE predictions predict a decreasing spring-in with increasing thickness, the experimental results do not correlate with the predicted values.

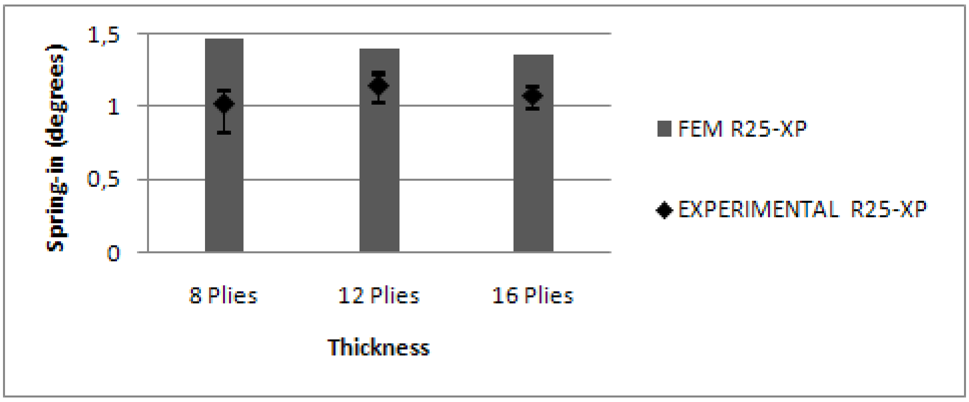

Figure 4.5. Effect of thickness on spring-in for the cross-ply parts with 25 mm radius.

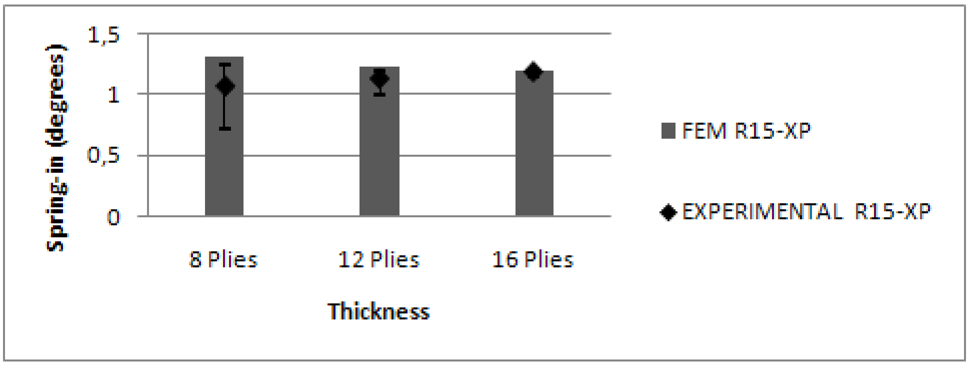

Figure 4.6. Effect of thickness on spring-in for the cross-ply parts with 15 mm radius.

4.2.1. Thickness Profile along the Length of Parts and Image Analysis

Thickness measurements were taken at seven stations along the length of the laminates using a micrometer with 3-digit sensitivity. The corner thickening can be seen easily from the thickness measurement along the length of the laminates in Figures 4.7 to 4.10. The thicknesses measured at seven stations indicated in Figures 4.7 to 4.10 are also listed in Table 4.2. The parts with 15 mm radius have greater corner thickening as compared to the parts with 25 mm radius and unidirectional parts had greater corner thickening as compared to cross-ply parts. Also, according to image analysis, fiber volume fraction of the corner of the 8 plies unidirectional laminate with 25 mm radius is 62.982 and the fiber volume fraction of the corner of the laminate with 15 mm radius is 52.812,which shows that resin flow occurs from the arm of the part to corner. The resin flow is low in cross-ply parts as compared to unidirectional parts. Also, the average fiber volume fractions for the parts are represented in Table 4.3.

These results show that in unidirectional parts the fibers in the bag side are bridging the corner resulting in resin flow into the corner and hence corner thickening. This effect is more pronounced in the tighter radius part (R15). Corner thickening results in higher resin fraction, higher through-the thickness CTEs and hence greater spring-in values

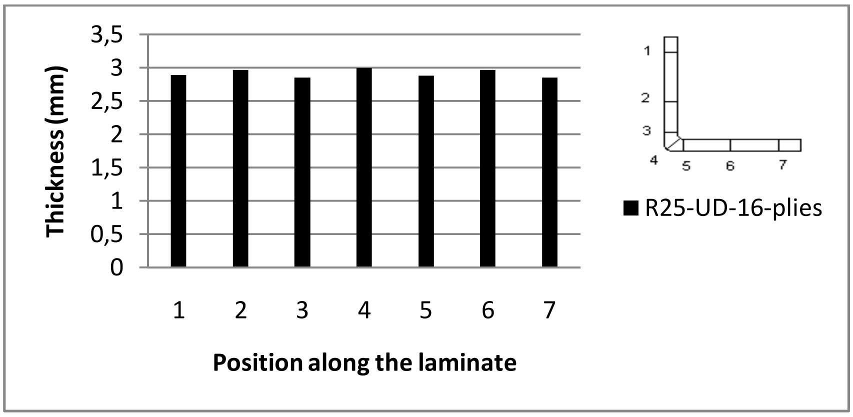

Figure 4.7. Thickness measurements along the length of 16 plies unidirectional laminate with 25 mm radius.

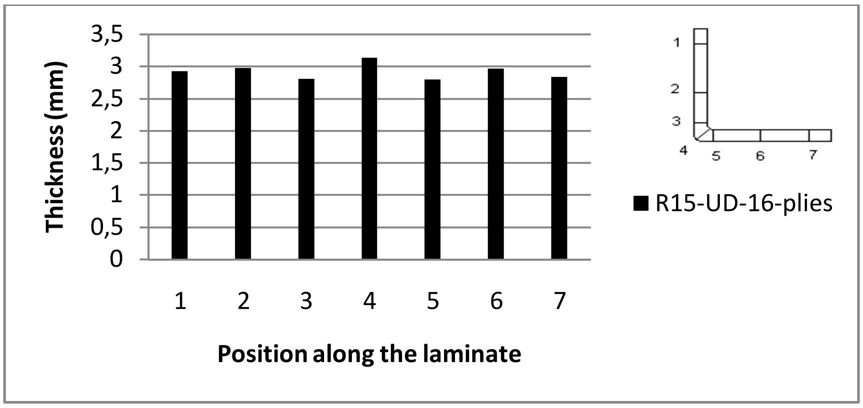

Figure 4.8. Thickness measurements along the length of 16 plies unidirectional laminate with 15 mm radius.

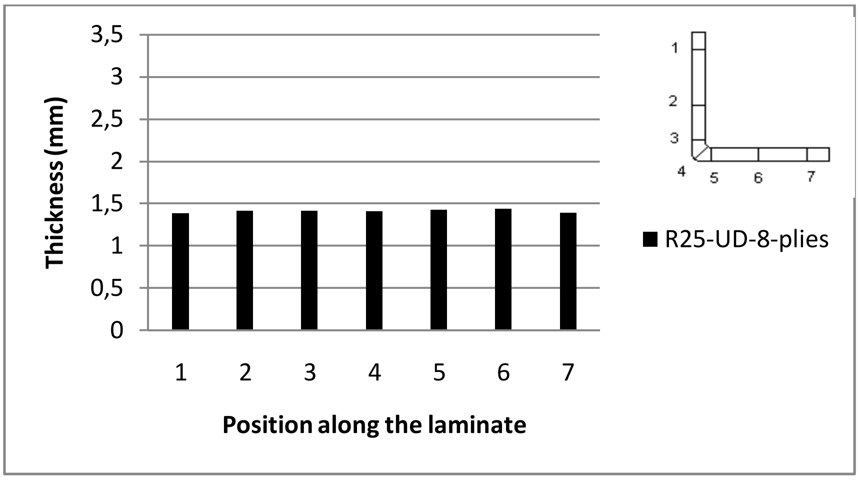

Figure 4.9. Thickness measurements along the length of 8 plies unidirectional laminate with 25 mm radius.

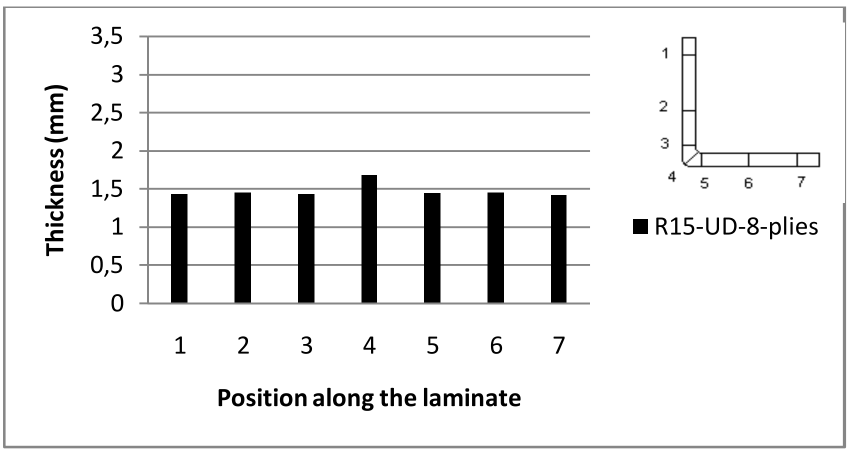

Figure 4.10. Thickness measurements along the length of 8 plies unidirectional laminate with 15 mm radius.

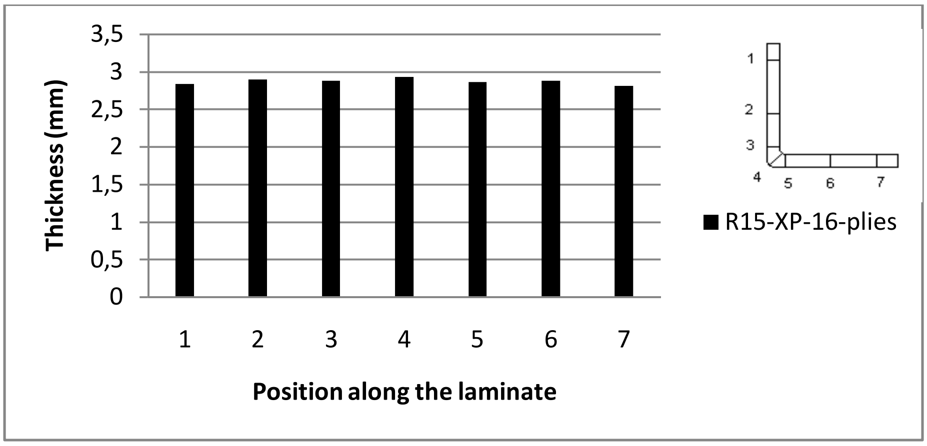

Figure 4.11. Thickness measurements along the length of 16 plies cross-ply laminate with 15 mm radius.

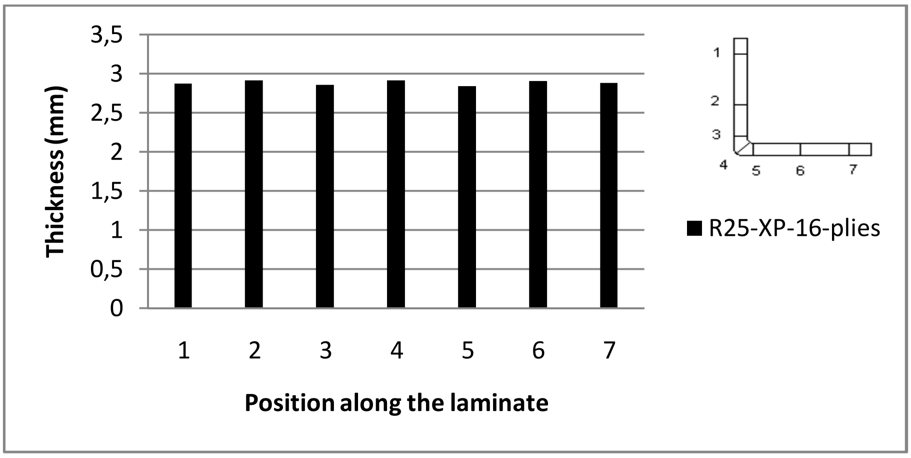

Figure 4.12. Thickness measurements along the length of 16 plies cross-ply laminate with 25 mm radius.

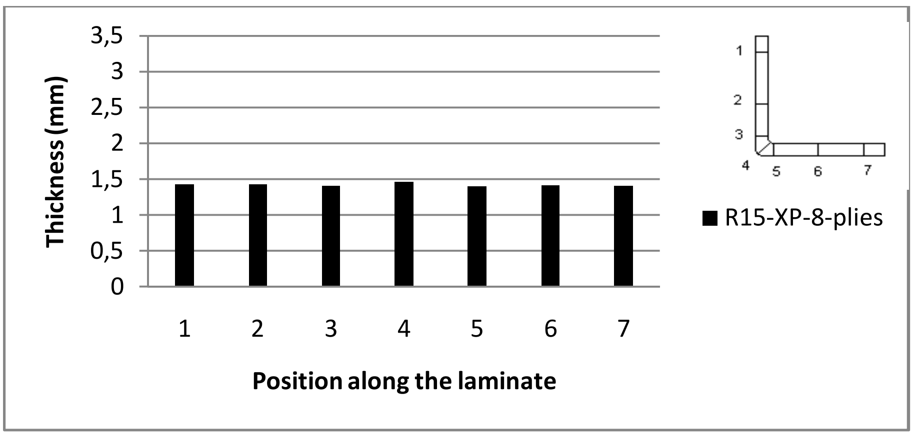

Figure 4.13. Thickness measurements along the length of 8 plies cross-ply laminate with 15 mm radius.

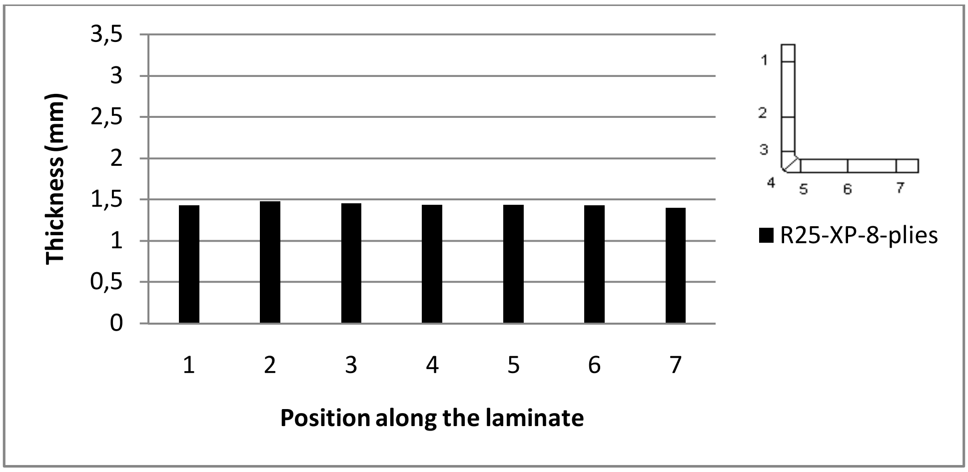

Figure 4.14. Thickness measurements along the length of 8 plies cross-ply laminate with 25 mm radius.

Table 4.2 Thickness measurements along the length of the parts.

Position	R15-UD-16-plies	R15-XP-16-plies	R25-XP-16-plies	R25-UD-16-plies
	(mm)	(mm)	(mm)	(mm)
1	2.92	2.84	2.869	2.883
2	2.973	2.897	2.908	2.963
3	2.806	2.876	2.85	2.852
4	3.131	2.931	2.912	2.991
5	2.796	2.866	2.84	2.873
6	2.96	2.877	2.904	2.964
7	2.831	2.813	2.879	2.845
	R25-XP-12-plies	R25-UD-12plies	R15-XP-12-plies	R15-UD-12-plies
1	2.085	2.019	2.144	2.18
2	2.122	2.162	2.157	2.208
3	2.194	2.1	2.159	2.128
4	2.171	2.163	2.202	2.354
5	2.192	2.086	2.136	2.121
6	2.186	2.163	2.099	2.219
7	2.16	2.105	2.059	2.088
	R15-UD-8-plies	R15-XP-8-plies	R25-UD-8-plies	R25-XP-8-plies
1	1.433	1.426	1.383	1.43
2	1.457	1.421	1.419	1.47
3	1.435	1.403	1.414	1.447
4	1.68	1.46	1.41	1.438
5	1.448	1.402	1.42	1.433
6	1.46	1.42	1.436	1.423
7	1.422	1.404	1.39	1.394
	R25-XP-4-plies	R15-UD-4-plies	R25-UD-4-plies	R15-XP-4-plies
1	0.735	0.698	0.725	0.738
2	0.759	0.716	0.727	0.726
3	0.72	0.722	0.738	0.716
4	0.721	0.74	0.721	0.732
5	0.74	0.708	0.731	0.718
6	0.733	0.715	0.744	0.736
7	0.731	0.715	0.738	0.721

Figure 4.15. Photomicrograph at 50x magnification from the corner of the 8 plies unidirectional laminate with 25 mm radius (no-bleed condition)

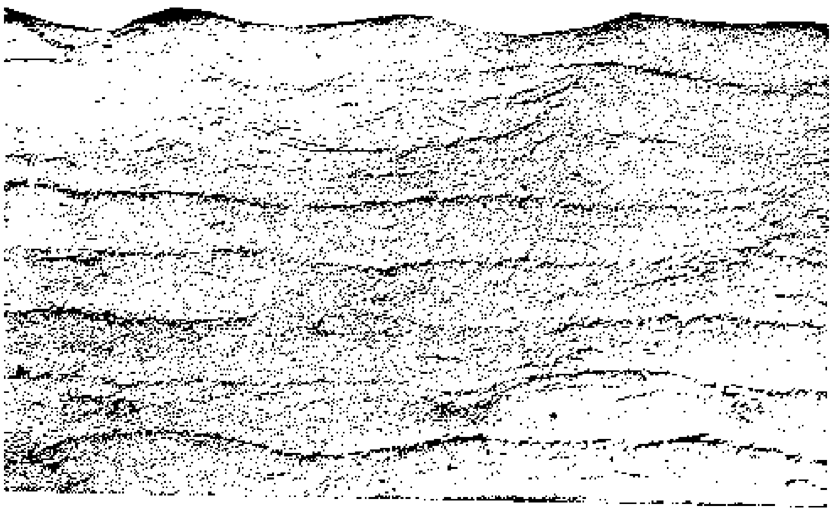

Figure 4.16. Binary image of photomicrograph (Figure 4.15)

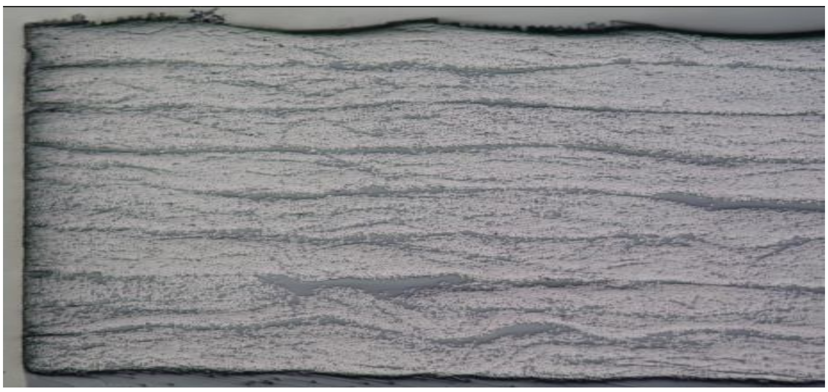

Figure 4.17. Photomicrograph at 50x magnification from the corner of the 8 plies unidirectional laminate with 15 mm radius (no-bleed condition)

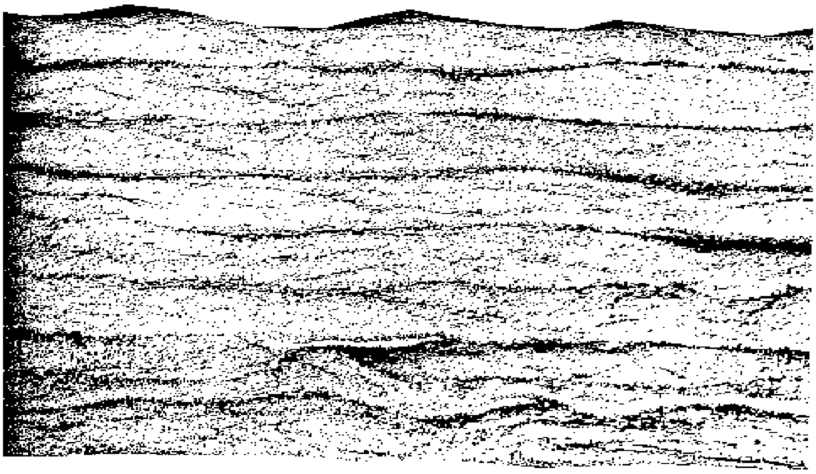

Figure 4.18. Binary image of photomicrograph (Figure 4.17)

Table 4.3. Average fiber volume fraction of the parts.

R15-UD-4 plies	65.28
R15-XP-4 plies	64.25
R25-UD-4 plies	65.31
R25-XP-4 plies	64.83
R15-UD-8 plies	63.78
R15-XP-8 plies	62.65
R15-UD-12 plies	61.93
R15-XP-12 plies	61.60
R25-UD-12 plies	62.79
R25-XP-12 plies	61.17
R15-UD-16 plies	60.46
R15-XP-16 plies	60.08

4.2.2. Corner Deformation of the Part in the Finite Element Model

The interface stresses between tool and the part due to the mismatch of the CTE of the part and the tool cause tension stress during the first and second step. When the part vitrifies these stresses are locked, and causes deformation of the part to conform to its final shape after the part is released from the tool and cools down to the room temperature. The cross sections where the stresses are plotted are shown in Figure 4.19 together with the local coordinate systems at the curved and flat sections.

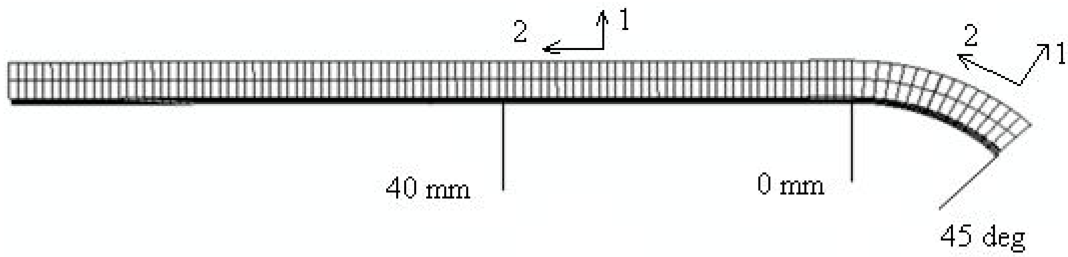

Figure 4.19. Representation of section where stresses (σ22) taken.

According to numerical results taken from the FE Model solution at the end of the second step, the nominal stress σ_{22} increased towards the corner of the part. It takes its maximum value at 45 deg (symmetry line). This showed that corner consolidation could not perform well and the bag side fibers loaded excessively in the viscous and rubbery state, then when the part vitrified stresses remain in the part. Deformations occur as the part removed from the tool. σ_{22} values at the end of second step are higher at the bag side fibers in cross-ply parts as compared to the unidirectional parts. This also explains that cross-ply parts give more spring-in than the unidirectional parts. Moreover, the fiber stress (σ_{22}) values at the inner side for 8-ply and 16-ply unidirectional parts are comparable but these values are less effective in the thicker parts because the thicker parts have higher bending stiffness as compared to the thinner ones. As a result thinner parts bend more than the thicker ones.

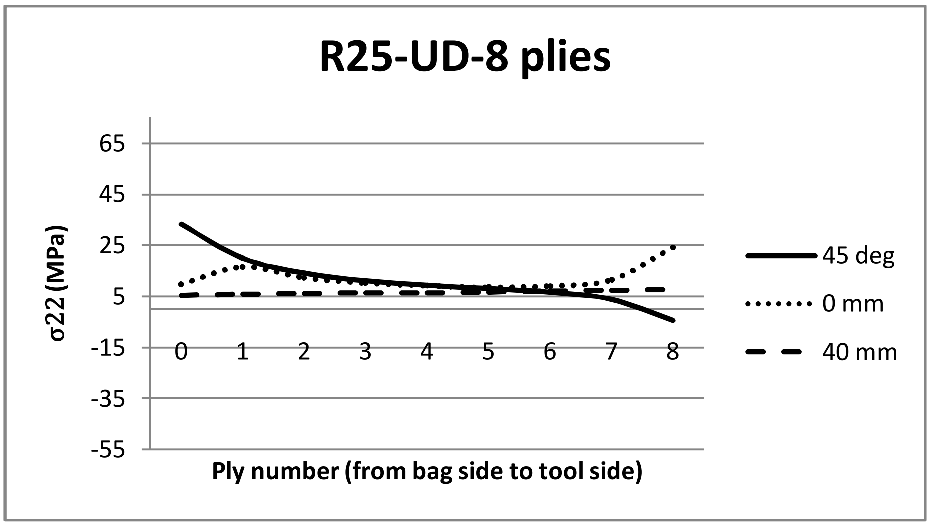

Figure 4.20. Through thickness σ_{22} stress for R25- UD-8 plies part

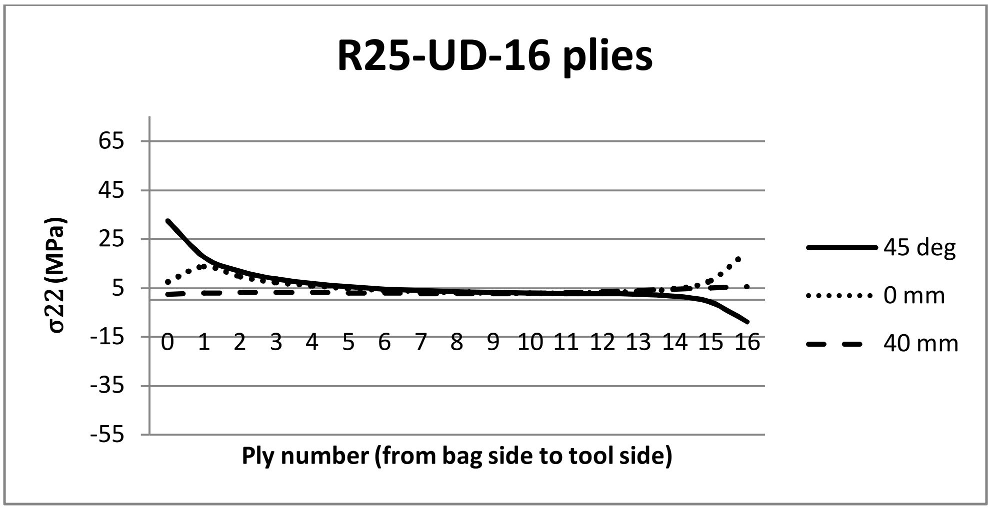

Figure 4.21. Through thickness σ_{22} stress for R25- UD-16 plies part

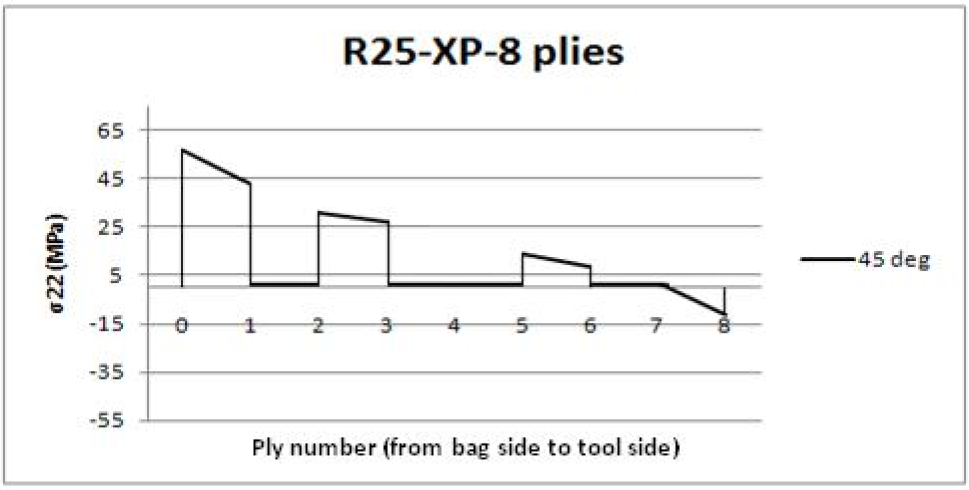

Figure 4.22. Through thickness σ_{22} stress for R25- XP-8 plies part

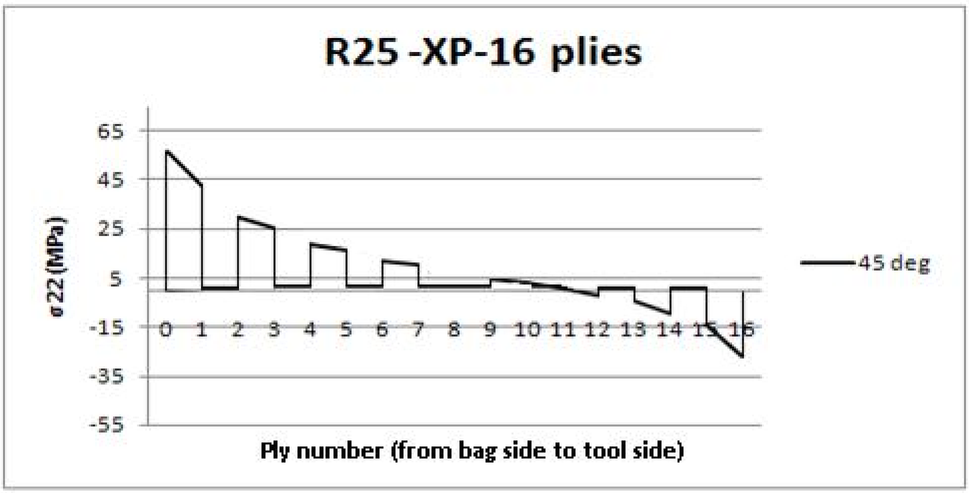

Figure 4.23. Through thickness σ_{22} stress for R25- XP-16 plies part

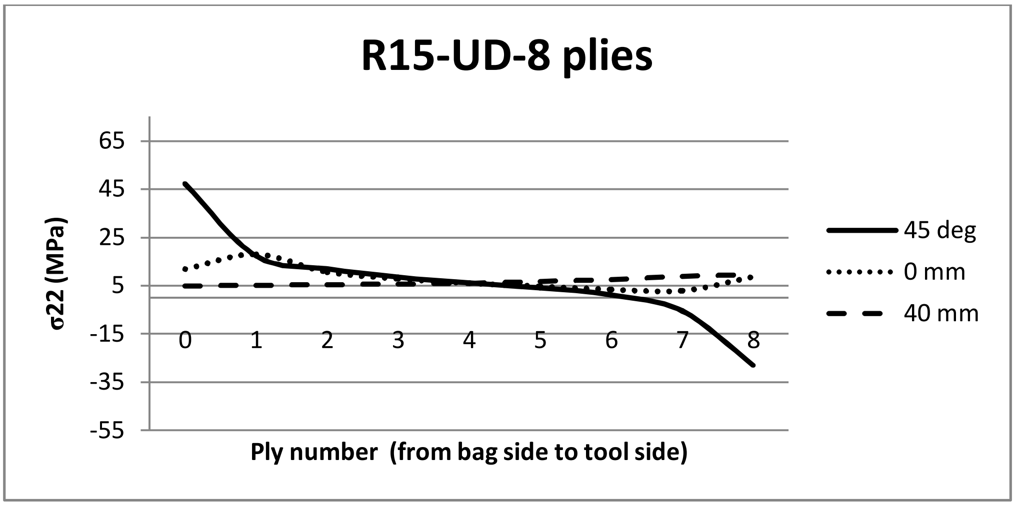

Figure 4.24. Through thickness σ_{22} stress for R15-UD-8 plies part

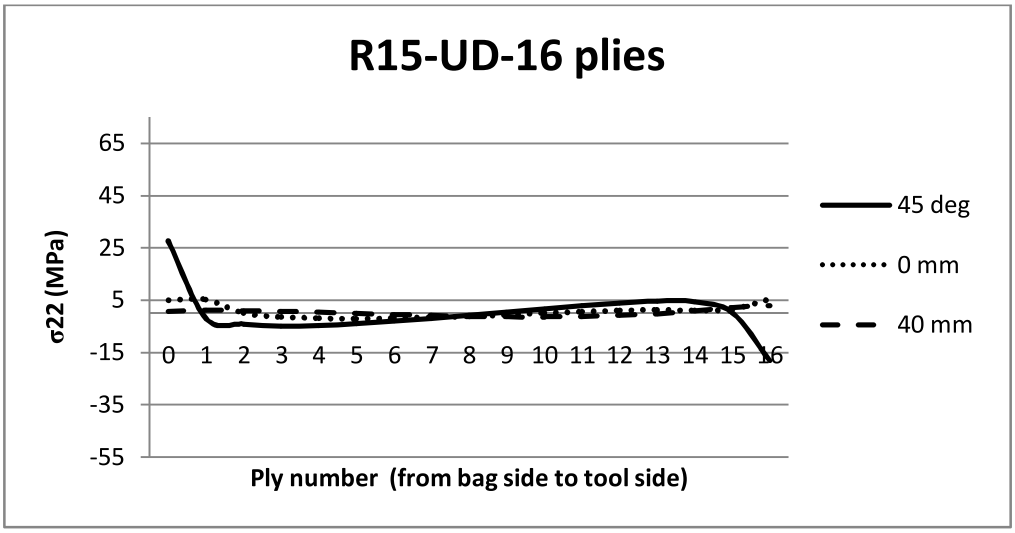

Figure 4.25. Through thickness σ_{22} stress for R15-UD-16 plies part

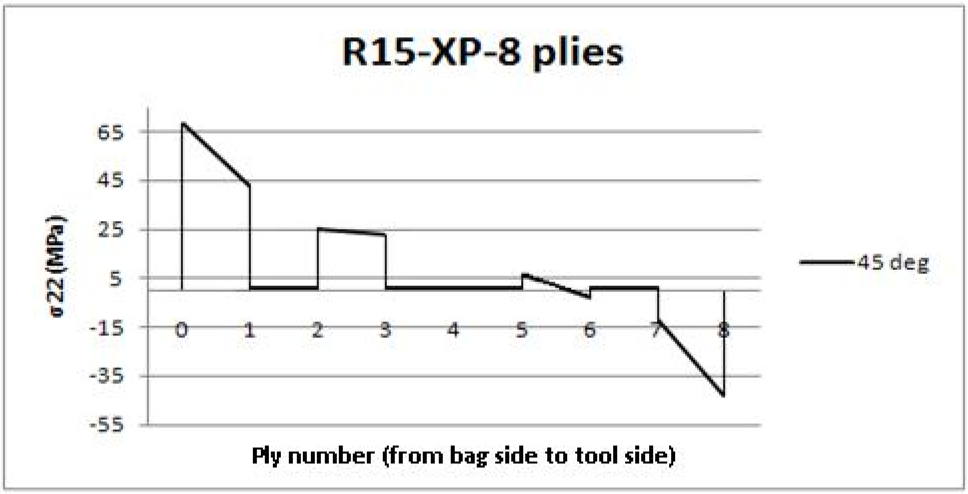

Figure 4.26. Through thickness σ_{22} stress for R15-XP-8 plies part

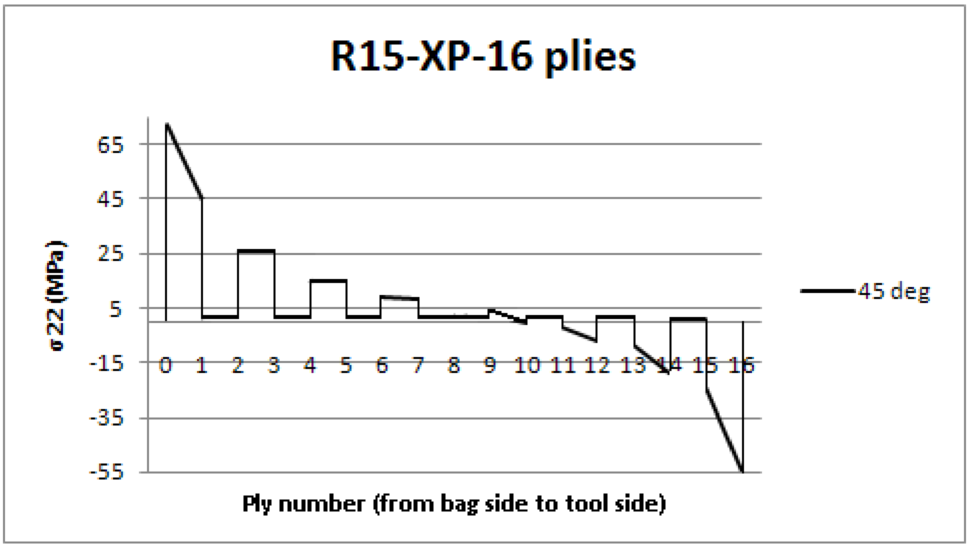

Figure 4.27. Through thickness σ_{22} stress for R15-XP-16 plies part

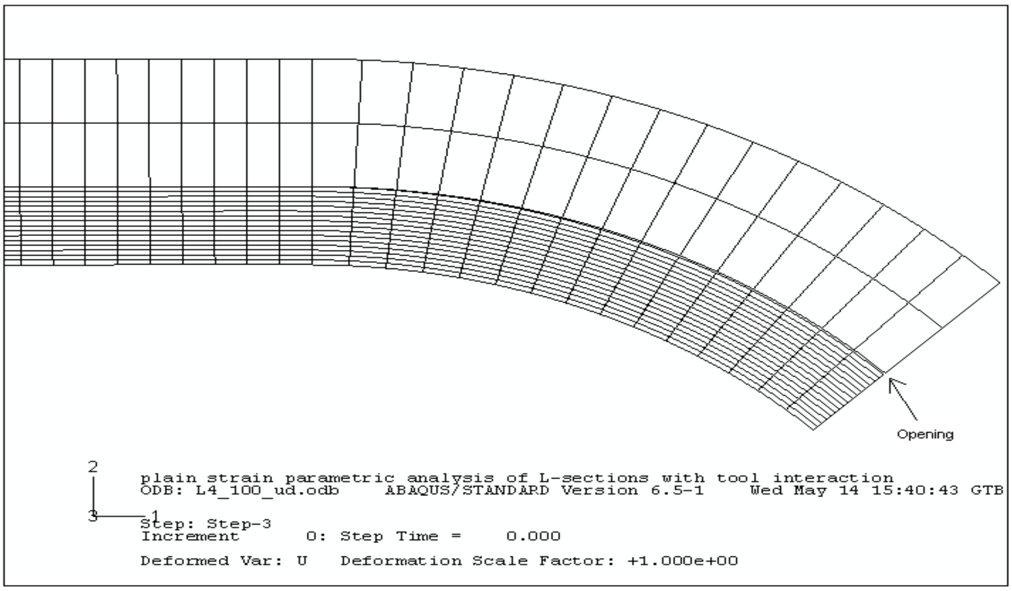

Figure 4.28. The finite element model of the 16 plies unidirectional part with 25 mm radius

As seen in Figure 4.28, the finite element model showed that opening occurs at the corner of the L-shaped parts, which results from cure shrinkage in the second step of the model and fiber bridging of the corner. The monitored opening value is higher in the parts with 15 mm radius as compared to the parts with 25 mm radius, as illustrated in Figure 4.29 and Figure 4.30. In Figure 4.29 and Figure 4.30 the autoclave pressure (CPRESS), frictional shear stress (CSHEAR), separation from the tool (COPEN), and relative displacement between the tool and the part (CSLIP) are shown at the end of Step 2 for the unidirectional parts. The autoclave pressure is ineffective at the corner of the part due to fiber bridging, which causes the part to disengage from the tool at the corner. Experimental results confirm this opening by corner thickening. The opened region at corner is filled by resin so that the thickness of the part at the corner increases. The corner thickness of the parts with 15 mm radius is greater than the parts with 25 mm radius so that cure shrinkage is higher in the parts with 15 mm parts. It can also be seen that in Figure 4.29 and 4.30 slipping with constant shear stress prevails for most of the interface at arms.

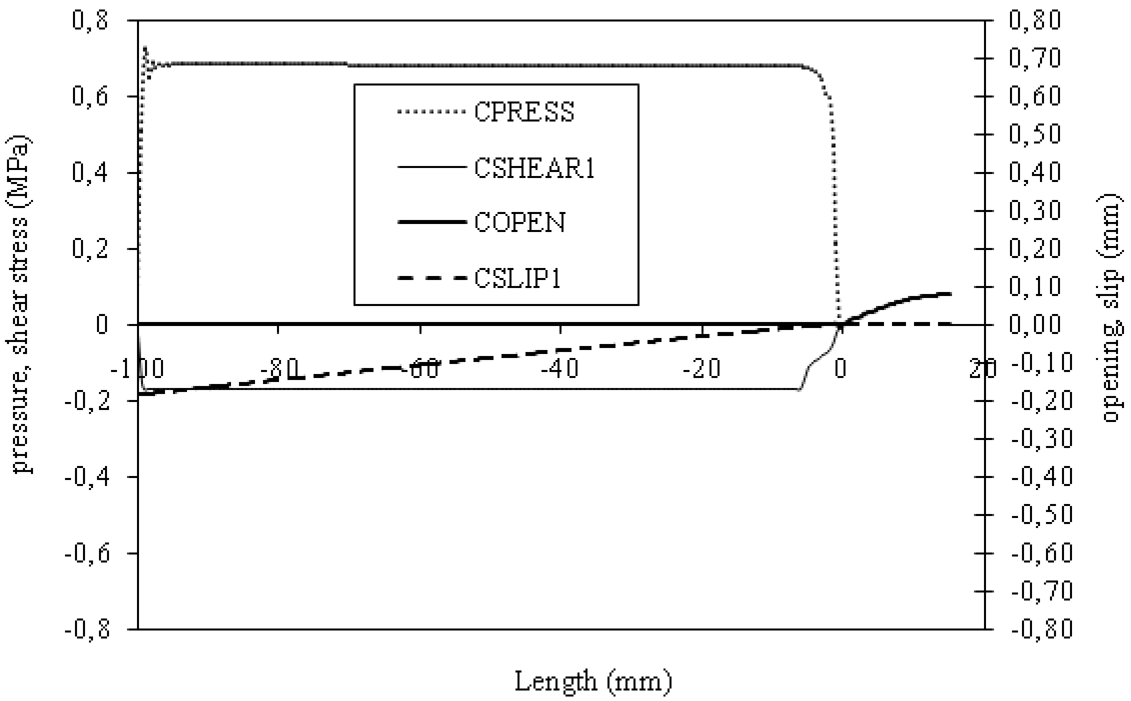

Figure 4.29. Stresses and displacements for the 16 plies unidirectional part with 25 mm radius

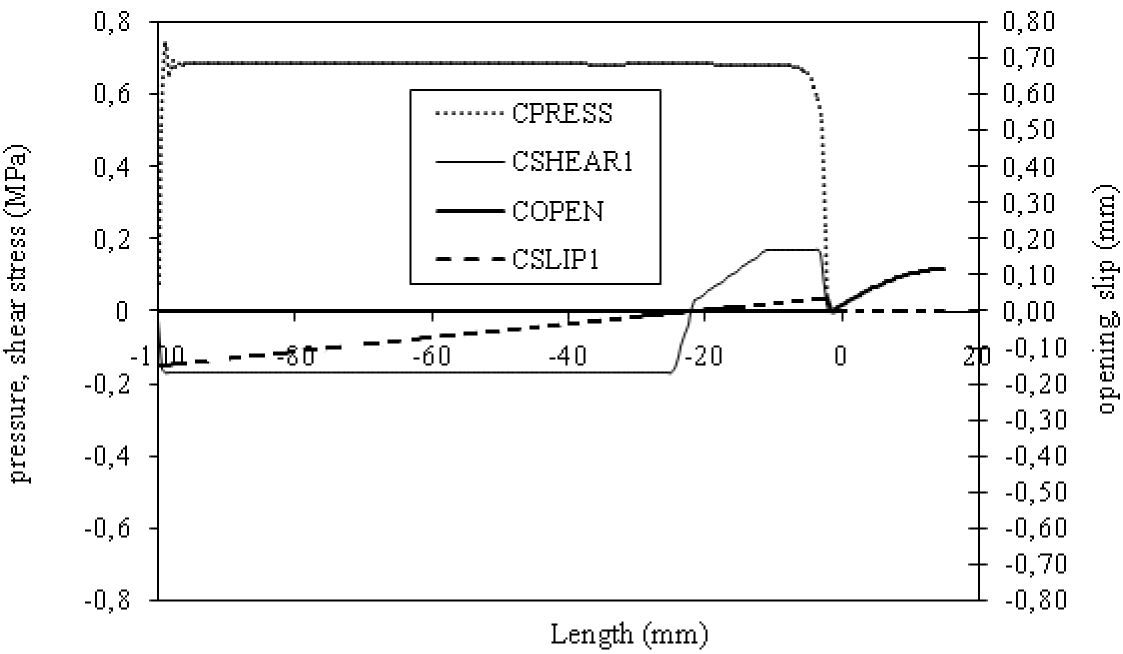

Figure 4.30. Stresses and displacements for the 16 plies unidirectional part with 15 mm radius

4.3. Corner Radius Effects

The measured and predicted spring-in values for the unidirectional parts are seen in Figure 4.31. 25 mm radius gives more spring-in than 15 mm radius for unidirectional stacking parts. According to the thickness measurement along the laminate, corner thickening is higher in the parts with 15 mm radius than the 25 mm ones for unidirectional parts.

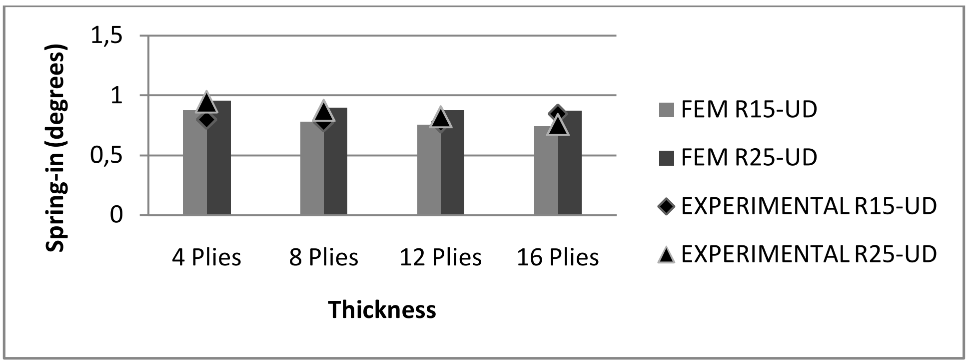

Figure 4.31. Corner radius effect on spring-in for the unidirectional parts

In the cross-ply parts, corner thickening in 15 mm radius and 25 mm radius is small as compared to the unidirectional parts so the corner thickening effect can be neglected in cross-ply parts. Measured values in Figure 4.32 confirm that.

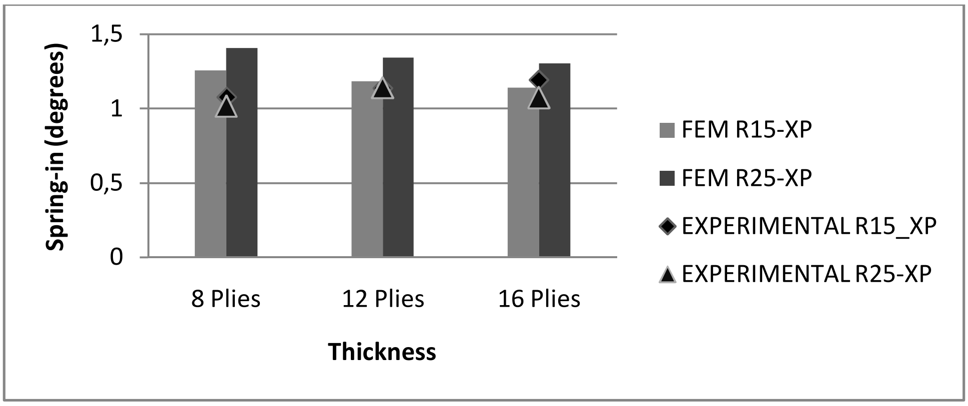

Figure 4.32. Corner radius effect on spring-in for the cross-ply parts

5. CONCLUSIONS AND FUTURE WORK

The effect of design parameters such as stacking sequence, thickness of the part, and corner radius on spring-in was investigated. For this purpose an innovative and flexible tool is designed which enables production of high quality L- and U-shaped parts. The tool itself can be pressurized, so it doesn't require an autoclave. It also enables flexible curing schedules due to very low thermal inertia of the system. The tool enables production of L-Shaped parts with two corner radii, i.e., R15 and R25 mm parts. Hence the effect of several design parameters on spring-in was investigated. The Manufacturer's Recommended Cure Cycle (MRCC) is adopted and kept fixed, while changing the design parameters such as lay-up, thickness, and corner radius.

The obtained results are summarized:

- The manufactured mold and the lamination process worked very well. According to image analysis, the produced composite laminates do not include any voids or impurities.

- For the effect of ply-orientation, cross-ply laminated parts have greater spring-in than unidirectional parts. The through-the thickness CTE and cure shrinkage of the cross-ply parts are greater than the unidirectional ones, which results from the constraints imposed by fibres in the two in-plane directions in cross-ply parts. For unidirectional parts, predicted spring-in values closely match the measured spring-in values but for the cross-ply parts, the finite element analysis slightly over-predicts the spring-in values.

- As for the effect of thickness on spring-in, it was observed that for the unidirectional laminates thin parts give high spring-in as compared to thick parts (except R15-UD-16 plies part). This trend was not observed for cross-ply laminates.

- Image analysis and thickness measurements reveal that the parts with 15 mm radius have greater corner thickening as compared to 25 mm radius parts, and unidirectional parts had greater corner thickening as compared to cross-ply parts. In the tooling with larger radius, the prepregs conformed to the raidus more easily, but in the smaller radius tooling, the autoclave pressure was not effective at the corner due to fiber bridging and the resin flow from the arms to the corner resulted in corner thickening.

- 25 mm radius gives more spring-in than 15 mm radius for unidirectional parts. In the cross-ply parts, corner thickening in 15 mm radius and 25 mm radius was small as compared to the unidirectional parts so the corner thickening effect can be neglected in cross-ply parts.

- Finite Element Analysis showed that the fibers in the inner radius of the L-Shaped parts experience significant fiber stresses during the molding. These stresses are rearranged as the part is released from the tool and cools down, contributing to the spring-in.

- The autoclave pressure is not effective at the corner region due to fiber bridging and this results in disengagement of the part from the tool during curing, and resin flow from the arms to the corner, resulting in corner thickening.

As a future work,

- In the experimental setup, the use of breather absorbed the excess resin from the parts so that cure shrinkage effect and the effect of through-the thickness CTE were reduced and fiber volume fraction was increased. The breather may be eliminated to examine the effect of higher cure shrinkage and higher through-the thickness CTE in the parts.

- The finite element model consisted of three steps: viscous, rubbery and glassy state. However, the mechanical properties of the resin were assumed to be same in first two states. To take into account the effect of viscous properties of the resin in the model, first step has to be changed by determining viscous properties of resin. Most of the fiber movements in the resin occur at the viscous state so fiber stresses minimize.

However in the present study this effect was neglected so higher spring-in values in cross-ply parts can be depend on this phenomenon.

- Inter-ply slip may be added to code to approach the actual mechanism of shape conformation of laminates in the corner.

- Moreover, corner thickening effect may be added to the code by increase the cure shrinkage and CTE at the corner of the parts.

- For the tool-part interaction, friction coefficient can be determined for the release film on a steel tool. The maximum shear stress value used in the model should be determined again for steel tooling.

- The 2-D finite element model may be transferred to 3-D finite element model to examine the effect of third direction.

REFERENCES

1. Garstka, T., "Seperation of Process Induced Distortions in Curved Composite Laminates", PhD Thesis, University of Bristol, 2005

2. Mazumdar, S.K., "*Composites Manufacturing"*, CRC Press, Florida, 2002.

3. Albert, C., and Fernlund, G., "Spring-in and Warpage of Angeled Composite Laminates", *Composite Science and Technology* 62 (2002) 1895-1912, 2002.

4. Ersoy, N., Potter, K., Wisnom, M., and Clegg, M., "An Experimental Method to Study the Frictional Processes during Composites Manufacturing", *Composites*: Part A36 (2005) 1536-1544

5. Radford, D.W., and Rennick, T.S., "Separating Sources of Manufacturing Distortion in Laminated Composites", *Journal of Reinforced Plastics and Composites*, Vol.19, No.08/2000

6. Fernlund, G., Poursartip, A., Twigg, G., *A Review of Tool-Part Interaction in Composite Processing*, The University of British Columbia

7. Wisnom, M., R., Gigliotti, M., Ersoy, N., Campbell, M., and Potter, K., D., "Mechanisms Generating Residual Stresses and Distortion during Manufacture of Polymer-Matrix Composite Structures", *Composites*: Part A 37 (2006) 522-529

8. Fernlund, G., Rahman, N., Courdji, R., Bresslauer, M., Poursartip, A., Willden, K., and Nelson, K., "Experimental and Numerical Study of the Effect of Cure Cycle, Tool Surface, Geometry, and lay-up on the Dimensinol fidelity of Autoclave-Processed Composite Parts ", *Composites*: Part A 33 (2002) 341-351.

9. Radford, DW., and Diendorf, RJ., "Shape Instabilities in Composites Resulting from Laminate Anisotropy", *Journal of Reinforced Plastics and Composites*, 12:58-75, 1993.

10. Huang, C., K., and Yang, S., Y., "Warping in Advanced Composite Tools with Varying Angles and Radii ", *Composites*: Part A 28A (1997) 891-893

11. Yoon, K.J., and Kim,J.S., "Effect of Thermal Deformation and Chemical Shrinkage on the Process Induced Distortion of Carbon/Epoxy Curved Laminates", *Journal of Composite Materials*, Vol. 35, No. 03/2001

12. Suska, J., and Tschirnich, J., "Intercomparison of Thermal Expansion Etalons", *Euromet Project 390, PTB Final Report section* 5.22B, Berlin-Friedrichshagen, 1999

13. Benzie, M.A., "Investigation of Springback Associated with Composite Material Component Fabrication", *MSFC Center Director's Discretionary Fund Final Report*, Project 94-09, 1997

14. Derek Hull, An Introduction to Composite Materials, Cambridge University Press, New York, 1981.

15. Ersoy, N., Potter, K., Wisnom, M., R., and Clegg, M., J., "Development of Spring-in Angle during Cure of a Thermosetting Composite", *Composites*: Part A 36 (2005) 1700-1706

16. Svanberg, J., M., and Holmberg, J., A., "An Experimental Investigation on Mechanisms for Manufacturing Induced shape Distortionss in Homogeneous and Balanced Laminates", *Composites*: Part A 32 (2001) 827-838

17. Wisnom, M., R., Potter, K., D., and Ersoy, N., "Shear-lag Analysis of the Effect of Thickness on Spring-in of Curved Composites", *Journal of Composite Materials*, Vol. 41, No. 11/2007

18. Darrow, D.A., and Smith, L.V., “Isolating Componenets of Processing Induced Warpage in Laminated Composites”, *Journal of Composite Materials*, Vol. 36, No.21,21/2002

19. Ersoy, N., Potter, K., and Wisnom, M., R., “Modelling of the Spring-in Phenomenon in Curved Parts Made of a Thermosetting Composite”, to be published

20. Hubert, P., and Poursartip, A., “Aspects of the Compaction of Composite Angle Laminates: An Experimental Investigation”, *Journal of Composite Materials*, Vol. 35, No.01/2001

21. Johnston, A., Vaziri, R., and Poursartip, A., “A Plane Strain Model for Process-Induced Deformation of Laminated Composite Structures”, *Journal of Composite Materials*, Vol. 35, No. 16/2001

22. Svanberg, J., M., Altkvist, C., and Nyman, T., “Prediction of Shape Distortions for a Curved Composite C-spar”, *Journal of Reinforced Plastics and Composites* 2005; 24; 323

23. Svanberg, J., M., and Holmberg, J., A., “Prediction of Shape Distortions. Part II. Experimental Validation and Analysis of Boundary Conditions”, *Composites*: Part A 35 (2004) 723-734

24. Ersoy, N., Garstka, T., Potter, K., and Wisnom, M. R., “Development of the Properties of a Thermosetting Resin and Its Carbon Fiber Composite through Cure”, *Composite* Part A, in press.

25. Hibbit, Karlson, and Sorensen Inc. ABAQUS Online Documentation, Version 6.5-1; 2004.

26. HexPly 8552 Epoxy matrix, Product Data, Hexcel Composites

27. Cann, Michael., Adams, O., Schneider, C., "Characterization of Fiber Volume Fraction Gradients in Composite Laminates", *Journal of Composite Materials* 2008; 42; 447

28. Yang, Heechun, and Colton, Jonathan, "Quantitative Image Processing Analysis of Composite Materials", *Polymer Composites*, Val, 15, No.1, February 1994